Journal of Materiomics 10 (2024) 218–233

Contents lists available at ScienceDirect

Journal of Materiomics

journal homepage: www.journals.elsevier.com/journal-of-materiomics/

Review paper

Review of current $ZT > 1$ thermoelectric sulfides

Fu-Hua Sun [a, f, 1], Hezhang Li [b, c, *, 1], Jun Tan [a], Lingmei Zhao [a], Xinyu Wang [a], Haihua Hu [d], Chao Wang [c], Takao Mori [b, e, **]

[a] School of Materials Science and Engineering, Hubei Normal University, Huangshi, 435002, China
[b] International Center for Materials Nanoarchitechtonics (WPI-MANA), National Institute for Materials Science (NIMS), Namiki 1-1, Tsukuba, 305-0047, Japan
[c] Department of Precision Instrument, Tsinghua University, Beijing, 100084, China
[d] State Key Laboratory of New Ceramics and Fine Processing, School of Materials Science and Engineering, Tsinghua University, Beijing, 100084, China
[e] Graduate School of Pure and Applied Sciences, University of Tsukuba, Tsukuba, 305-8671, Japan
[f] Foshan Xianhu Laboratory of the Advanced Energy Science and Technology Guangdong Laboratory, Foshan, 528225, China

ARTICLE INFO

Article history:
Received 25 April 2023
Received in revised form
26 May 2023
Accepted 28 May 2023
Available online 20 June 2023

Keywords:
Synthetic technology
Figure merit of *ZT*
Sulfides
Thermoelectric

ABSTRACT

Thermoelectrics has played a fascinating role in the developments of direct energy conversion technologies. Over the past decade, sulfur-based thermoelectric materials have been significantly advanced in optimizing electrical and thermal transport due to their similarities in chemical and structural properties with tellurides and selenides. This review provides research progress on metal sulfides, particularly focuses on materials exhibiting high thermoelectric figure of merit ($ZT > 1.0$). It highlights the potential compounds, *e.g.* Cu–S, Sn–S, Pb–S based, and polysulfides. Great strategies of superionic conducting, band configuration tuning, high-entropy alloying, and anomalous harmonic scattering are try to demonstrate the performance-improved mechanisms for thermoelectric sulfides. In addition, some common synthesis recipes are briefly introduced, and thereby making potential candidates as excellent alternatives for producing thermoelectric power generators in the mid temperature. Key outcomes along with how to further improve the thermoelectric performance and promote its scale-up applications are also outlined at the end.

Contents

* Corresponding author. International Center for Materials Nanoarchitechtonics (WPI-MANA), National Institute for Materials Science (NIMS), Namiki 1-1, Tsukuba, 305-0047, Japan.
** Corresponding author. International Center for Materials Nanoarchitechtonics (WPI-MANA), National Institute for Materials Science (NIMS), Namiki 1-1, Tsukuba, 305-0047, Japan.
E-mail addresses: lihezhangshishui@163.com (H. Li), MORI.Takao@nims.go.jp (T. Mori).
[1] These authors contributed equally.

https://doi.org/10.1016/j.jmat.2023.05.011

1. Introduction

Thermoelectric (TE) technology, namely the capacity of directly converting energy from heat to electricity and vice versa, provides a great potential in the fields of harvesting waste heat and solid state cooling [1–5]. It possesses great merits, *e.g.* durability, modulability, emission-free, long lifetime, and low maintenance [6–8]. Despite notable progress [9,10], the implementation of TE practical application is still limited by its low conversion efficiency, which is determined by the dimensionless figure of merit $ZT = S^2\sigma T/\kappa$, where S is the Seebeck coefficient, σ is the electrical conductivity, κ is the thermal conductivity, and T is the absolute temperature, respectively. κ can be mainly divided into two parts: lattice (κ_L) and carrier (κ_e) contributions.

Enhancing ZT requires a trade-off between the inversely related electrical (α and σ) and thermal transport (κ), making it difficult to improve any individuals without degrading the others. $ZT > 1$ has served as a historical standard for niche application for a given TE material [11]. Generally, the dominating factors for achieving high ZT target either to increase power factor ($PF = S^2\sigma$) or to decrease κ. For example, band structure engineering [12] near the Fermi level (E_F) has been proved to be one of the effective way to improve PF due to the optimized charge carrier transport behaviors. Of course, κ is also related to the carrier concentration (n). Therefore, the search for good TE materials is all about finding a material with the suitable electronic and atomic structures. It is well described by a quality factor B [13]. B is a function of the number of band valley N_v and the inertial effective mass m_I^*. Increased N_v means larger number of conduction pathways for charged carriers to participate in electrical performance. Decreasing m_I^* ($= m_B^*$ is band effective mass for an isotropic structure) through maximizing electronic mobility ($\mu \propto \tau/m_I^*$, where τ is the scattering relaxation time), receives a strengthen electronic scattering. Therefore, large N_v directly leads to a real enhancement of B and thereby ZT. Great strategies, *e.g.*, nanostructure engineering [14–17], entropy engineering [18], rattling atoms [19], hierarchical architectures [20], defect engineering [21,22], and exploring novel compounds [23] have been well performed to reduce κ_L. These technologies instruct important findings of various state-of-the-art TE materials and achieving high ZT, including Mg_3Bi_2 ($ZT = 1.2$) [24], (Sn,Cd)$Te_{0.88}Se_{0.12}$ ($ZT = 0.9$) [25], (Pb,Sb,Ge)Se ($ZT = 1.54$) [26], $(Bi,Sb)_2Te_3$ ($ZT = 1.86$) [27], $Cu_2(S,Te)$ ($ZT = 2.1$) [28], (Na,Eu,Pb)Te ($ZT = 2.2$) [29], (Pb,Sr)Te ($ZT = 2.5$) [30], GeTe ($ZT = 2.7$) [31] and SnSe crystal ($ZT = 2.8$ [32] and even over 3.0 [33]).

Despite high ZT being achieved in aforementioned TE materials, most of them contain rare-earth and toxic elements and/or technical challenges, which probably hinders large-scale practical applications. Therefore, developing alternative materials composed of eco-friendly and low-cost elements with acceptable performance is very essential [34,35]. Noted that sulfur abundance on land hugely exceeds that of tellurium, enabling metal sulfides to become attractive candidates for TE community. Compared with tellurides, high phonon vibrational frequency derived from light sulfur atom leads to low intrinsic κ_L. From another perspective, in order to find effective strategies to achieve high ZT in TE sulfides, optimizing PF has become the core issue. For example, it attempts to reduce the bandgap (E_g) between anion- and cation-derived orbitals. The optimized electronic structure provides more efficient orbital overlap and the broadened bands, thereby reducing m_I^* and increasing μ. That is why the partial substitution of sulfur by selenium is successful in fine-tuning electrical transport properties in sulfides, and thereby reaching high ZT.

As represented in Fig. 1, the majority of high-performance TE sulfides are p-type semiconductors. n-type counterparts are very rare, and corresponding ZT-enhancement remains a challenge. It generally occurs in lead-based sulfides or compounds with complex crystal structures and/or multiple phases existence. Although the rocksalt-structured PbS, regardless of p- and n-type derivatives, achieves high ZT (reach and even exceed 1.0), increasing attentions on environmental impact of lead has been concerned. It prompts much investigation of the base-metal sulfides. As expected, tin chalcogenides derived from a single crystalline SnS, $ZT > 1.5$ [36], have recently motivated a wider investigation in TE community. In addition, several high-performance p-type polysulfides with earth-abundant elements were reported at moderate temperatures, $ZT > 1.0$, *e.g.*, tetrahedrites [37,38], colusites [39], chalcopyrites [40–42] and homo-structure sulfides [43]. For binary sulfides, p-type copper sulfides and their derivatives exhibit the exceptional TE properties, a peak ZT ~2.3 was achieved [44], which originated from the high mobility of Cu-cation. That is, the cation sub-lattice probably enters the liquid-like state, and induces phonon-liquid-electron-crystal (PLEC) type phases [45]. Noted that cation migration may promote compositional changes and even format secondary phases during preparation or processing, lead to introduce an instability into the matrix and cause cracking and loss of TE properties. Therefore, great efforts of introducing additional cations or finding alternative structures have been motivated in order to overcome the ionic diffusion and further block the migration path. Taking an overall view, volatilization in sulfur-based TE materials may also result in materials degradation and performance deterioration at increasing temperature. In favorable case, these faults (interfaces, boundaries or defects) can enhance phonon scattering and thereby reduce κ_L, which improves ZT value.

This review intends to prospect the merits of metal sulfides from the superionic conductivity, band configuration tuning, and anomalous harmonic phonon scattering, and high-entropy alloying aspects. It discusses some of the most promising binary sulfides and polysulfides, and underlies their TE properties-improved mechanisms. Considering great progress in the implementation of TE technology, huge efforts on capturing TE sulfides should be followed by studies highly reliable devices. Therefore, several fabrication technologies of TE sulfides are outlined. The future perspective and outlook about the material performance-enhancement and scale-up application are also given at the end.

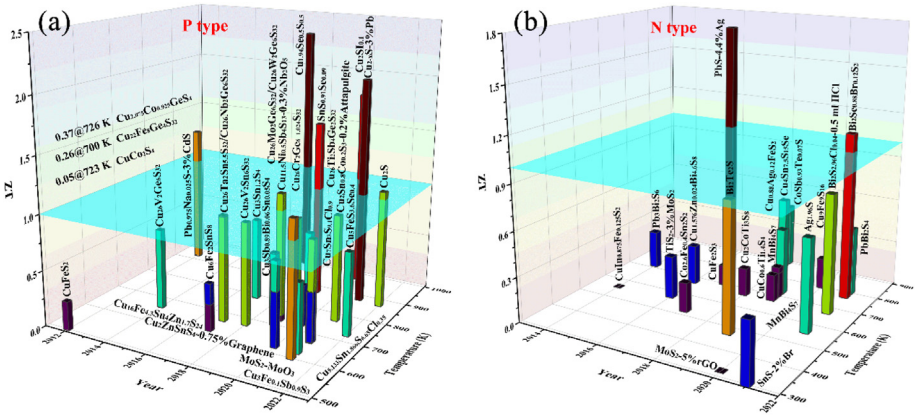

Fig. 1. Collections of peak *ZT* along with years and optimal temperature regions in both (a) p- and (b) n-type thermoelectric sulfides. All related references to $ZT > 1$ are listed in subsequent tables, while $ZT < 1$ contains Cu-M1-S (M1 = Sn [46–50], Sb [51,52], Fe [53–59], Zn [60], Co [61], Bi [62]), colusites [37,63–71], M2-S (M2 = Ag [72], Sn [73],Bi [74], Ti [75], Mo [76]), M3-Bi–S (M3 = Pb [77,78], Mn [43], Fe [43], Te [79]), and other alloys [80].

2. Structural merits for sulfide thermoelectrics

The strong linkage of metal sulfides to thermoelectricity originates from the work of M. Telkes [81] in 1950, who studied the TE properties (primarily electrical conductivity and Seebeck coefficient) of several sulfides in mineral forms. Although the lighter sulfur atom presents great challenges in achieving high performance which is typically attained in good materials with heavy atoms, the unique chemical and crystal structures can be exploited to synthesize materials with exceptionally high *PF* and low κ. And thereby it has received great attention in the TE landscape.

2.1. Superionic conduction of thermoelectric sulfides

Copper sulfides, particularly digenite $Cu_{2-x}S$ ($0 \le x \le 1$), are simply composed of two elements, but numerous intermediate phases have been found [82], varying from Cu-rich Cu_2S to Cu-poor CuS. According to the Cu–S phase diagram (Fig. 2a), $Cu_{2-x}S$ undergoes three phase transitions with increasing temperature, from monoclinic structure (γ phase) at room temperature (RT) to hexagonal (β phase) at $T \sim 376$ K, and then to cubic (α phase) at high temperature (HT). Zhang *et al.* [83] clearly reported the temperature-dependent crystal structures of $Cu_{2-x}S$ through HT X-ray diffraction (XRD). It is well indicated that, as shown in Fig. 2b, the hot-pressed $Cu_{1.8}S$ pellet displayed a complex phase transition from the combination of $Cu_{1.96}S$ (tetragonal structure) and Cu_2S (monoclinic) to a mixture of hexagonal Cu_2S and rhombohedral $Cu_{1.8}S$ at $T \sim 400$ K, and then to cubic Cu_2S at temperature around 820 K.

In low temperature (LT), monovalent Cu vacancies act as p-type dopants in $Cu_{2-x}S$. Cu vacancies can reduce the antibonding character, lower the energy position of the valence band maximum (VBM), and thereby enlarge the band gap (E_g) [85]. In typical cubic structure (HT, α phase), S atoms form ordered and rigid sublattice, functioning as the framework, while Cu atoms are disordered and split into tetrahedra sites. Cu ions occupy each tetrahedron randomly [86]. The d_{Cu} bands comprising the VBM are degenerate at Γ point, and the s_{Cu} bands, which can be considered to be the lowest CB, lie slightly below it at Γ point [87]. Therefore, Cu vacancies mainly shift down E_F and do not change the general shape of the band in $Cu_{2-x}S$ compound. That is, the shapes of the VB are immune to the Cu vacancies (LT and α phases) and Cu disorder (α phase). And thereby *n* can be safely tuned by the Cu vacancy content, which will be probably promote the diffusion of Cu ions, resulting in the liquid-like behavior and subsequent superionic conduction (SIC). Indeed, as previous report [88], the α phase is a classic superionic phase having freely mobile Cu ions, while β phase is a solid-liquid hybrid phase with Cu in a liquid-like substructure.

SIC has played a fascinating role in the development of TE materials. Based on thermodynamic study, the normal-to-SIC phase transition indicates that the entropy change per atom is similar to that half of the crystal state, namely the Cu sublattice is quasi-molten [89]. In SIC state (mainly α phase), the liquid-like sublattice is expect to hinder the heat transport by transverse mode phonons or lattice vibrations, and thereby the volumetric specific heat (C_v) is lower than that of the Dulong-Petit limit [90] ($3Nk_B$, *N* and k_B are the total number of atoms and Boltzmann constant, respectively). At the same time, the fixed sublattice provides a crystalline pathway for electronic transport. Regardless of copper sulfides, another SICs with good TE values have also been explored, *e.g.*, Ag–S alloys [91], Ag–Cu based sulfides [92], $AgBi_3S_5$ [93], and $CuTi_2S_4$ [70]. As for an inorganic semiconductor, α-Ag_2S received large attention due to its unusual ductility and respectable TE property. Fig. 2c describes the electronic band structures of α-Ag_2S using a PBE (Perdew, Burke, and Ernzerh) exchange-correlation functional [84]. α-Ag_2S is a direct bandgap semiconductor of E_g ~1.1 eV, and Fermi level is mainly formed by $4d_{Ag}$ and $3p_S$ orbitals. The energy barrier between Ag_I at tetrahedral site and Ag_{II} of the octahedral site is very small, presenting easily diffuse, especially at HT. In addition, the anti-bonding Ag–S states appear below E_F result in a structural phase transition, tending to SIC. These features of metal sulfides make a reduced κ_L while preserving high σ, which leads to a significant TE enhancement.

Beyond the SIC structures, TE properties are also significantly optimized and improved by entropy engineering [94] because material's entropy is a gene-like performance indicator. Increasing entropy works as an effective guide to improve microscopic configuration that may enhance the crystal structure symmetry, especially for matrix materials having low symmetry structures, *e.g.* $Cu_{2-x}S$-based substituted multicomponent compounds (LT phases). From the viewpoint of thermoelectrics, more elements are always recommended due to multi-scale phonon scattering theory. In addition, the element distributions should be uniform, and no secondary phases can be found in order to maintain high electrical properties. When the configurational entropy is high enough, all multicomponent materials tend to possess a high symmetry structure. This is well confirmed by a symmetry transition of high-entropy $Cu_2S_{1/3}Se_{1/3}Te_{1/3}$ [95], increasing from the monoclinic

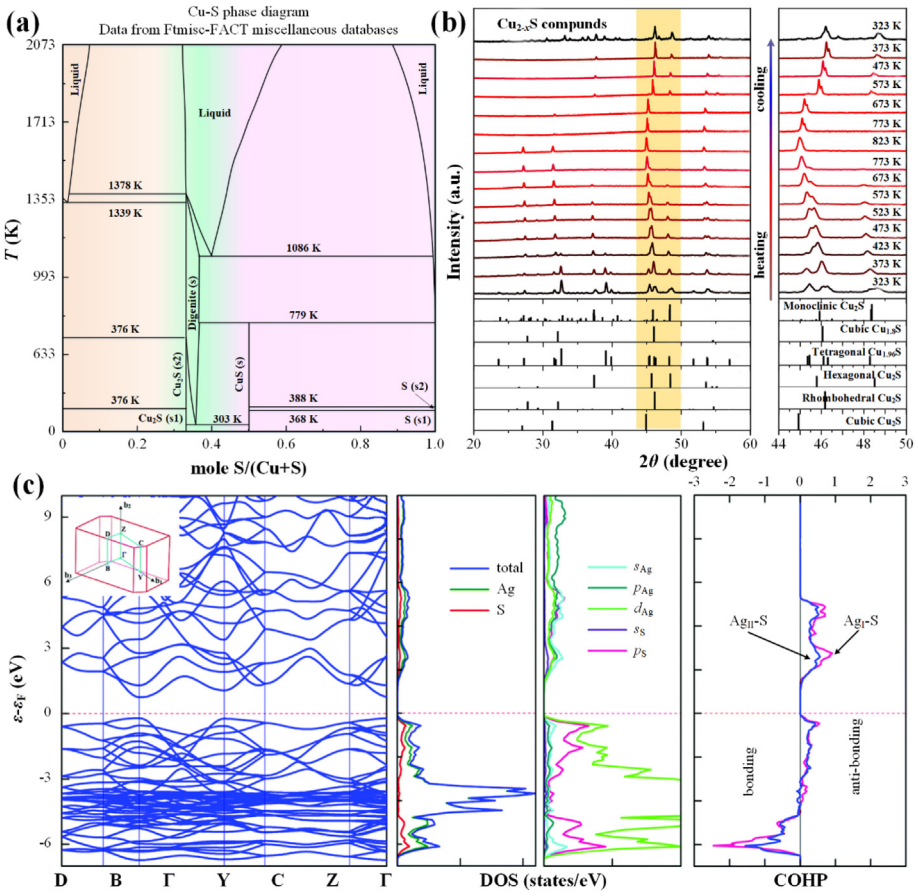

Fig. 2. (a) Cu–S phase diagram presents a series of copper-based sulfides in a narrow sulfur ratio of 30%–50%(in mole). (b) The XRD patterns of $Cu_{2-x}S$ crystals at temperature increased from RT to 823 K and then decreased to 323 K. Reprinted from Ref. [83], Copyright (2021), with permission from Elsevier Ltd. (c) Band structure and total/partial-DOS of α-Ag_2S in the first-Brillouin zone, and the COHP data of Ag–S bonding. E_F is referenced at the top of the VB. Reprinted figure with permission from Ref. [84], Copyright (2013) by the Royal Society of Chemistry.

structure to hexagonal at RT when the configurational entropy is above 0.6 k_B f.u.$^{-1}$. High symmetry crystal structures generally have a high band convergence or overlapped bands near the E_F due to the high symmetry inducing more equivalent positions in both real and reciprocal space. This can significantly increase the electronic density-of-states (DOS) and effective mass (m^*), and thereby enhance S. Competitive TE performance was obtained in $Cu_5Sn_{1.2}MgGeZnS_9$ [96], in which the additional Sn plays an important role in tuning n and improving S.

2.2. Band configuration tuning

Trying to tune the band parameters [97] in metal sulfides has led to a fruitful strategy to analyze their complex band structures. It can be engineered either by modifying the relative energy of the electronic bands through alloying or by introducing impurity energy levels that are resonant with the host band through resonant doping.

Lead sulfide (PbS) is a typical member of lead chalcogenides, known as a promising high-performance TE material. Its valence band is easily regulated, and thereby the band alignment was achieved with suitable M(4)S (M(4) = Cd, Zn, Ca, Sr and *etc.*) [98]. Simultaneously, carrier scattering is largely suppressed by reducing carrier transport barriers. As shown in Fig. 3a, a high energy barrier was caused by the large energy difference (energy offset ΔE) between the conduction bands (CBs) of PbS and M4S. For p-type case, the degree of hole scattering scales with the size of the valence band offsets, and decreases with increasing temperature due to thermal band broadening. ΔE exceeds the magnitude of thermal energy k_BT at HT. It is very useful to facilitate carrier transmission across the interface and further modify the carrier mobility in p-type PbS. The intrinsic band structure is a direct band gap in L point with valence band (VB) contributed from S 3p and CB from Pb 6p in PbS. However, alloying (like Sn atom) and incorporating with dopant (like PbTe compound) [99] can sharpen the CB shape and narrow the band gap in n-type PbS, as well as make the CB position fine alignment, as displayed in Fig. 3b. These help to obtain high electron mobility (μ_H) and relatively high effective mass (m^*). Furthermore, element doping can introduce a gap state between the CB and VB or an extra CB (Ga/In doping [100]), which induces Fermi level pinning effect. For example, the Ga-doped PbS sets up a hybrid state, Ga 4s and S 3s-3p states, and the Fermi level lies within its gap states. Ga–In codoping also adds a In 5s state with a small electron energy difference of 0.03 eV at L and Γ points.

Tin sulfide (SnS) is a rising star in the TE community due to its fascinating electronic and acoustic transport features. SnS is a multiple band structure, and its large m^* mainly comes from the increased energy degeneracy (N_V). It is an effective way to shape the multiple band structures through alloying specific elements [36]. As shown in Fig. 3c, Se-doped SnS, the energy offsets have dropped dramatically over the sharpened VBs. It is also found that the VBs take on the temperature-dependent evolution behavior after Se alloying, including two-band divergence, convergence, and crossing with increasing temperature. The structure evolution of VB

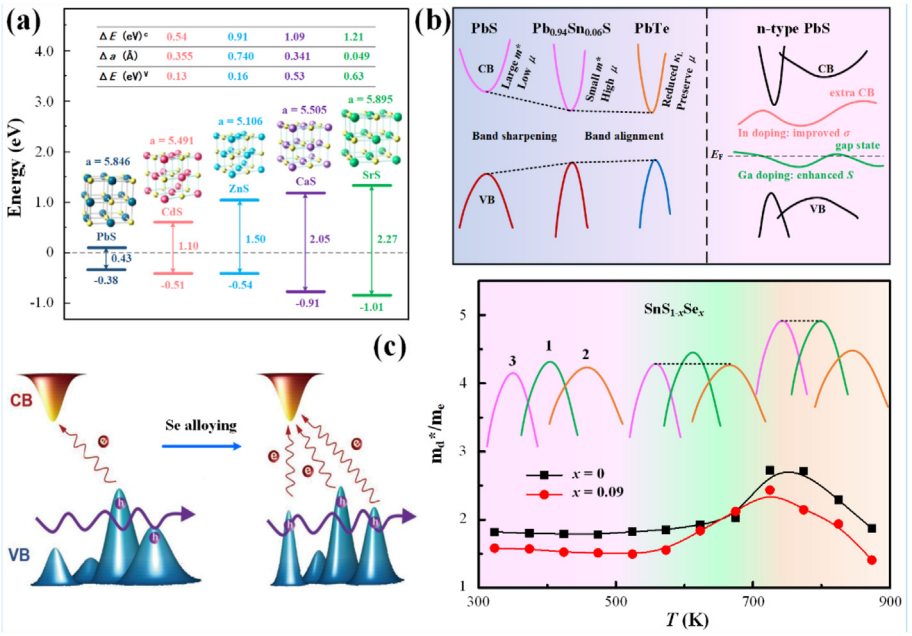

Fig. 3. (a) DFT band alignments of the CB and VB energy levels for PbS, CdS, ZnS, CaS, and SrS. Adapted by permission from Ref. [98], Copyright (2012) by the American Chemical Society. (b) Designed strategy to synergistically optimize carrier and phonon transport property in PbS with Sn/In/Ga alloying and PbTe incorporation. Reprinted figure with permission from Refs. [89,90], Copyright by the American Chemical Society. (c) Schematic diagram of electronic band structures for Se-doped SnS, and corresponding dynamic VBs evolution. Adapted by permission from Ref. [36], Copyright (2019) by the Authors, some rights reserved.

promotes the electrical transport property, which can be well evaluated through the weighted mobility μ_w ($\mu_w \approx \mu_H(m_d^*/m_e)^{3/2}$), herein the m_d^* and m_e are the density of states effective mass and the electron mass, respectively.

2.3. Anomalous harmonic phonon scattering

The CuS_4 tetrahedron is considered to be the building block or prototype for a variety of ternary and higher-ordered copper-based sulfides. The simple vertex linking of CuS_4 tetrahedra gives rise to a zinc blende network, in which ordered cations probably induce formation of supercells. $CuM(5)S_2$ (M(5) = Fe, Al, Ga, In, Tl and *etc.*) with a chalcopyrite structure adapts a vertex-linked feature. There is ordering of Cu (I) and M(5) (III) cations over 4-coordinate sites. Meantime, replacement of one half of M(5) cations produces a stannite structure exemplified by Cu_2ABS_4, tetrahedrons among CuS_4, AS_4 and BS_4 linking through their vertices. The antifluorite-type structure of $Cu_5M(5)S_4$ also generates a network of vertex-linked CuS_4, in which a statistical distribution of Cu cations and vacancies separates over the eight available tetrahedral sites.

Complex structures are also observed in copper-containing minerals, *e.g.*, colusites, tetrahedrites, famatinites. Colusite can be vertex-linked by CuS_4 and BS_4 tetrahedra, while the tetrahedrite is often considered as a complex defective derivative of zinc blende-like network. Each Cu_{12d} atom forms a tetrahedron with four S_{24g} atoms (as shown in Fig. 4a), and Cu_{12e} atom is linked with one S_{2a} and two S_{24g} atoms, forming a basic unit of CuS_3 trigonal plane. Sb atom is coordinated with three S_{24g} atoms as an SbS_3 trigonal pyramid. The interplay between electronic transport and crystal structure has been well provided by Long *et al.* [101] It is revealed that the Jahn-Teller driven electronic instability results in a marked reduction in the density of states at Fermi level (DOS patterns in Fig. 4b). The formation of molecular-like Cu–S cluster suppresses the carrier transport, and thereby the electronic conduction is compelled by variable-range-hopping mechanism among clusters. Lai *et al.* [102] further calculated the vibration DOS (VDOS in Fig. 4c) of all atoms at 300 K and 600 K. Both low- and high-energy modes were observed in the temperature dependent lattice parameters. The low-lying modes revealed quasilocalized sites and significantly weakened bonding (*i.e.* Cu_{12e}) due to their low frequency and energy. The calculated atomic displacement parameter (ADP) value ~ 0.143 2 $Å^2$ for tetrahedrite is much larger than Lindemann parameter, leading to a part-crystalline and part-liquid structure. This structural features displays some similarities with those of cage-based TE materials, such as skutterudites and clathrates.

3. High performance thermoelectric binary sulfides

A common electronic structural feature for above-mentioned sulfides resides in a hybridized VB derived from metal (*d*) and S (3*p*) orbitals. A high degeneracy of VB results in relatively high *S* and thereby PF. The appreciable SIC (particularly, copper and silver ion) in many of the complex structures may manifest itself either in relatively large ADPs or strong delocalization of cation-ions, leading to the sublattice atoms keeping a liquid-like state, which purposes a great effect on phonon transport.

3.1. Copper sulfide

Although stoichiometric copper sulfide (Cu_2S) is an intrinsic semiconductor, Cu deficiency easily leads to a p-type behavior. The carrier (hole, h^+) concentration dramatically increases with increasing Cu vacancies, leading to an enhanced σ and reduced *S*. However, the κ_L values are nearly independent with Cu-deficiency contents. As summarized in Table 1, a series of $Cu_{2-x}S$-based materials exhibits superior TE properties with high *ZT* ($\geq$1), which is a benchmark suggesting potential of materials suitable for applications at intermediate temperatures. Among them, a few peak *ZT* values, for example $Cu_{2-x}S$-3%Pb [83], can reach or even exceed 2.0 at HT.

It is found that Cu_{2-x}(Se,Te,S) can form a solid solution in composition ranges from half Se/Te and half S [25,102] or even

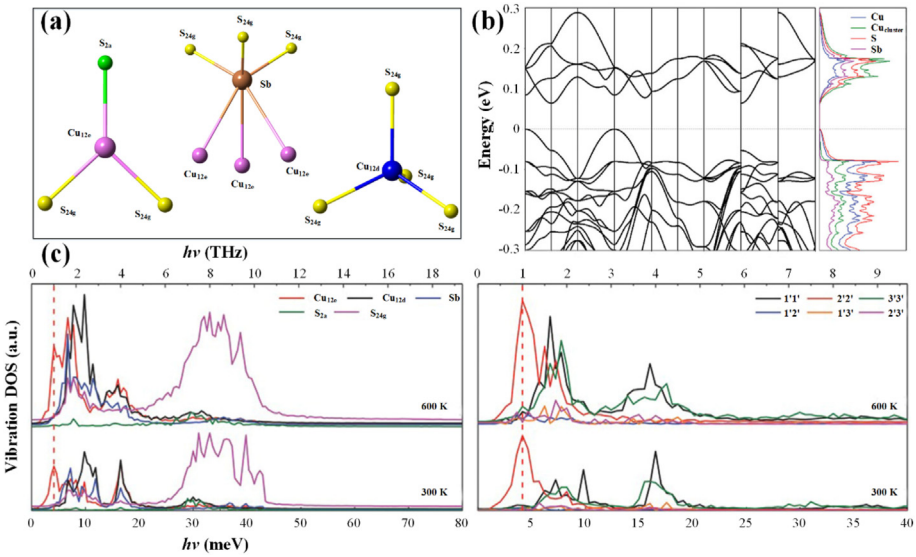

Fig. 4. (a) Crystallographic units of $Cu_{12}Sb_4S_{13}$ compound. (b) Electronic band structure and partial density of states for tetragonal $Cu_{12}Sb_4S_{13}$. Reprinted figure with permission from Ref. [101], Copyright 2020 by the WILEY-VCH Verlag GmbH & Co. KGaA, Weinheim. (c) Vibration density of states of isotropic motion for all atoms and anisotropic motion for Cu_{12e} atoms in $Cu_{12}Sb_4S_{13}$ at both 300 K and 600 K, respectively. Reprinted figure with permission from Ref. [102], Copyright 2015 by the WILEY-VCH Verlag GmbH & Co. KGaA, Weinheim.

Table 1
State-of-the-art thermoelectric properties of $Cu_{2-x}S$-based materials.

Material	T (K)	ZT_{max}[a)]	S (μV/K)	σ (10^4 S/m)	n_H[a)] (10^{20} cm^{-3})	μ_H[a)] (cm^{-2}·V^{-1}·s^{-1})	κ (W·m^{-1}·K^{-1})	κ_L (W·m^{-1}·K^{-1})	Synthesis method[a)]	Ref.
$Cu_{1.94}Se_{0.5}S_{0.5}$	1000	2.30	225	2.50	7.900	2.20	0.58	0.21	SSR + SPS	[44]
$0.31Cu_2S$-$0.69Cu_{1.96}S$	932	2.10	220	2.31	9.300	2.40	0.48	0.14	WC	[103]
$Cu_2S_{0.52}Te_{0.48}$	1 000	2.10	220	1.80	18.000		0.37		SSR + SPS	[28]
$Cu_{2-x}S$-3%Pb	880	2.03	198	2.90			0.49	0.19	HP	[83]
$Cu_{1.98}S_{1/3}Se_{1/3}Te_{1/3}$	1 000	1.90	248	1.80	11.200		0.60	0.30	SSR + SPS	[104]
$Cu_{1.97}S$	973	1.90	245	1.20			0.36		MS	[105]
$Cu_2SI_{0.1}$	973	1.80	220	1.85			0.50		RFIHP	[106]
$Cu_{1.97}S$	1 000	1.70	302	0.91	7.300	0.69	0.48		SSR + SPS	[90]
$Cu_{1.9}Mn_{0.1}S$	700	1.63	275	3.90	0.007		1.25	0.61	SSR + MA + SPS	[107]
$Cu_{1.8}S$-5%(in mass)$CoSb_3$	773	1.60	192	2.15			0.47		SSR + SPS	[108]
$Cu_{1.95}S$	800	1.56	321	1.40	2.300	6.11	0.66	0.46	FVIR	[109]
$Cu_{2-x}S$-0.75%Graphene	873	1.56	163	4.50	13.000	1.25	0.64	0.10	MA + SPS	[110]
$Cu_{1.9}Fe_{0.0325}S$	1 000	1.50	262	1.48	1.100	2.20	0.62	0.41	SSR + SPS	[111]
$Cu_{2-x}S$	710	1.41	248	1.70	0.600		0.62	0.33	HP	[112]
$Cu_{1.8}S$−3%In_2S_3	773	1.40	112	8.70	4.400		0.65	0.33	MA + SPS	[113]
$Cu_{1.94}S$	773	1.23	205	1.90	3.200	4.10	0.45	0.24	MA + SPS	[114]
Cu_2S−2%In_2S_3	850	1.23	198	2.65	2.400	5.80	0.98	0.47	SPS	[115]
$Cu_{1.8}S$−1%WSe	773	1.22	110	8.00	7.800	19.50	0.68		MA + SPS	[116]
$Cu_{1.8}Sb_{0.02}Sn_{0.03}S$	773	1.20	173	3.10	5.100	2.70	0.60		MA + SPS	[117]
$Cu_{1.95}S$−NaOH	833	1.10	212	2.20	80.000		0.71	0.41	WC + SPS	[118]
$Cu_{1.8}Na_{0.05}S$	773	1.10	112	7.53	59.500	26.90	0.76		MA + SPS	[119]
Cu_2S	873	1.07	275	0.80	1.100		0.47	0.37	CP	[120]
Cu_2S	873	1.07	270	1.07	2.300	1.40	0.47	0.36	MA + SPS	[121]
$Cu_{2-x}S$-0.25%C	773	1.04	191	1.70	1.300	5.80	0.47	0.22	WC + SPS	[122]
$Cu_{1.96}S$	773	1.01	230	1.60			0.68		HTS + MA + SPS	[123]
$Cu_{1.8}S$−1%Ru	773	1.00	120	9.00	4.500	14.50	1.05		MA + SPS	[124]
$Cu_{2-x}S$	800	1.00	152	4.10	2.300	8.28	0.75	0.19	WC + SPS	[125]
90%Cu_2S−10%Cu_5FeS_4	900	1.00	205	1.75			0.76		SSR + HP	[126]

[a)] ZT_{max} is the peak ZT at each optimal temperatures, n_H (n_e) and μ_H (μ_e) are hole (electron) concentration and mobility, SSR is solid state reaction, SPS is spark plasm sintering, HP is hot pressing, MS is melt solidification, RFIHP is radio frequency-introduced hot pressing, MA is mechanical alloying, FVIR is flash vacuum-induced reaction, WC is wet chemical method, CP is cold pressing, HTS is hydrothermal synthesis, respectively.

down to one third of Se/Te/S [104] using Cu_2S, Cu_2Se, and Cu_2Te nanocrystalline specimen. These solids are solved as hexagonal structures with space group $R\bar{3}m$. Actually, these compounds are quasi-single crystals consist of a variety of 10–30 nm mosaic grains (Fig. 5a), possessing a unique hierarchical microstructure composed of mesoscale polymorphs, nanoscale domains and modulations. Due to the absence of boundary or interface scattering, as presented in Fig. 5b, mosaic crystals have dramatic effects on the charge carrier and phonon transport behaviors. Combined with a low sound speed originating from the intrinsic liquid-like Cu ions at HT, an ultralow κ is achieved (almost 0.4 W·m^{-1}·K^{-1}, as shown in Fig. 5c). Furthermore, high PF values (PF_{max} = 13.2 μW·cm^{-1}·K^{-2}) are observed due to a high weighted mobility, which is similar to that of copper selenides [127]. All

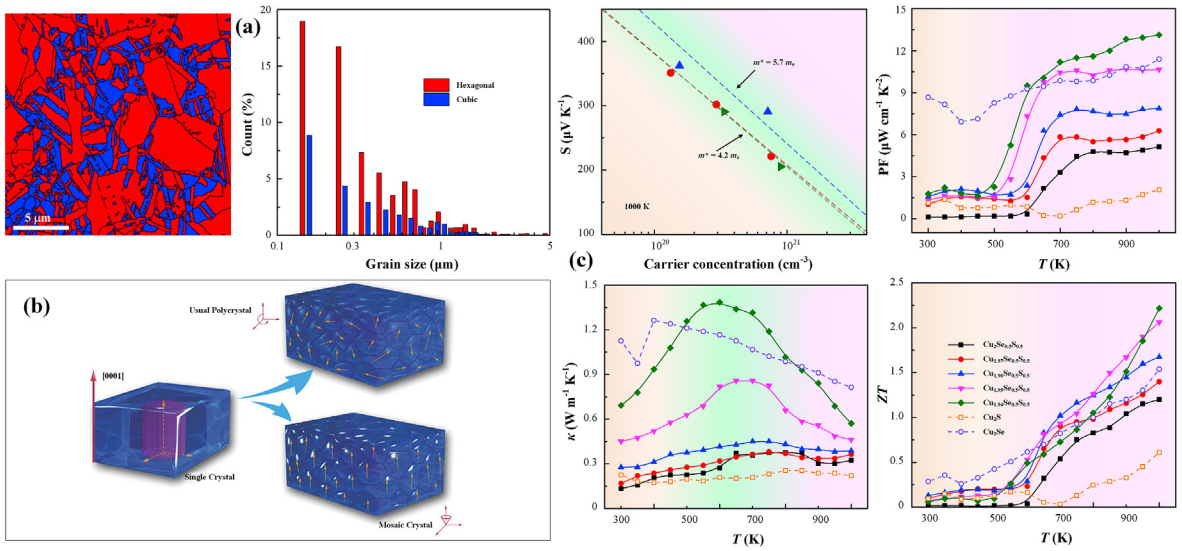

Fig. 5. (a) Phase mapping and grain size distribution in $Cu_2(Se,S)$ compound. (b) Structural characteristics of a single crystal, a usual polycrystal, and a mosaic crystal. Reprinted figure with permission from Ref. [28], Copyright 2015 by the WILEY-VCH Verlag GmbH & Co. KGaA, Weinheim. (c) Seebeck coefficient *S* as a function of Hall carrier concentration at 1 000 K, and temperature dependence of *PF*, *κ*, and *ZT* for Cu–Se–S compounds. Reprinted from Ref. [44], Copyright (2017), with permission from Elsevier Ltd.

favorable factors lead to an improved quality factor (*B*) and then TE properties in $Cu_{2-x}(Se,Te,S)$ compounds. Finally, a peak *ZT* value of 2.3 was received, which is the highest values in bulk polycrystalline sulfides.

Many studies focus on suppressing the phase transitions and Cu segregation for $Cu_{2-x}S$ compounds through alloying Cu sites with light atoms [107,117], introducing nano-inclusions, encapsulating thin carbon-shell $Cu_{2-x}S$@C [122] or $Cu_{2-x}S$@graphene [110], informing *in-situ* nanophases induced from In_2S_3 [115] or WSe [116], and dispersing nanoparticles of $Cu_{2-x}S$-Ru [124], Cu_2S–⊜ Cu_5FeS_4 [126] or $Cu_{2-x}S$-NaOH [118]. These composites show an evident improvement of both PF and *ZT* values due to simultaneously optimized *n* and reduced phase transition temperature. Along with the structure stabilization, sulfur volatilization and copper segregation, high TE performance together with large PF and ZT_{ave} [120] values in $Cu_{2-x}S$ will be beneficial to its practical applications in TE devices.

3.2. Lead sulfide

The quest to achieve high TE performance, low-cost and earth-abundant PbS remains an open opportunity to explore. Its property can be enhanced by tailoring the chemical bonding and modifying nanostructures. As compared to PbSe and PbTe, PbS has higher deformation potential at similar doping level due to the stronger electron-phonon coupling. The approaches of elaborately optimizing m^* and n_H to improve the electrical transport are well validated in PbS systems. Meanwhile, n_H optimization can effectively balance *S* and *σ*, and thereby produce a high average PF (PF_{ave}). Recently, as presented in Table 2, many efforts have been made to improve TE properties with *ZT* over 1.0 for n- and p-type PbS-based materials at optimal temperatures. n_H and κ_L have been well optimized by doping and nanostructuring, such as Na, K, Ag, Cu, Te doping or codoping, and/or Cd/Sr/CaS, Cu_2S nanostructuring *etc.* in p-type compounds. Zhao *et al.* [98,128,129] have investigated the effect of endotaxially nanostructured ZnS, CaS, CdS, and SrS on the TE properties of Na-doped p-type PbS in detail. Fig. 6a is a high-resolution transmission electron microscopy (HRTEM) image of the $Pb_{0.975}Na_{0.025}S$–3%CdS sample. The nanograin shows random distribution of irregularly sized precipitates. The average precipitate size is about 4 nm. It is confirmed that these nanostructures are lattice-matched, isostructural to PbS with endotaxially orientation. Furthermore, the elastic strain maps present pervasive stain field distribution in and around the precipitates. The line scanning profile shows a maximum 6% difference in lattice parameter at the phase interface. By means of a closely coupled phonon-blocking/electron-transmitting approach through embedding endotaxially nanostructured second phases in PbS system, as shown in Fig. 6b, *ZT* values are obviously improved in the entire temperature ranges. A record high *ZT* of ~1.3 in $Pb_{0.975}Na_{0.025}S$–3%CdS has been realized at 923 K (see Table 3).

Compared with p-type PbS, n-type materials face huge challenges in improving PF due to a single CB transmission, indicating that improvement through the well-known approaches (for example band convergence) is hardly possible. Hence, TE properties of n-type PbS-based alloys can be only enhanced from the perspectives of improving *σ* and lowering *κ*. Engineering certain electronic states [89,90] is the common strategies to enhance *σ*, and designing novel nanostructures [132,139] and/or multiple defects [146,134] can effectively suppress κ_L. Sometime, the secondary phase inclusions trigger a valence disproportionation [135] of metal cations, preserving high μ_H. Finally, an extraordinary *ZT* of 1.7 in n-type part was realized both $Pb_{0.93}Sb_{0.05}S_{0.5}Se_{0.5}$ [132] and PbS-4.4% Ag [133].

3.3. Tin sulfide

Sn-based sulfides came into the sight of TE researchers due to both high *σ* originating from the high in-plane carrier mobility and ultralow *κ* deriving from the strong lattice anharmonicity. Li *et al.* [151] successfully synthesized pristine SnS bulk using a simple MA + SPS method in 2014, and firstly reported a relatively high *ZT* of 0.16 at HT. They also revealed that the microstructure and TE properties were independent of the stoichiometric ratio and sintering temperature because of the decomposition of redundant S content in powder. Adjusting Na-doping content via wet chemical (WC) synthesis [152] leads to a state-of-the-art PF of 3.62 $\mu W \cdot cm^{-1} \cdot K^{-2}$ for the polycrystalline at 873 K, and thereby raises *ZT* value up to 0.52. Recently, it is found that heterovalent or monovalent cation doping (such as Na^+ [149] and Ag^+ [148]) in Sn

Table 2
State-of-the-art thermoelectric properties based on PdS materials.

Material	T (K)	ZT_{max}	$ZT_{ave.}$ [b]	S (μV/K)	σ (10^4 S/m)	n_H (10^{19} cm^{-3})	μ_H (cm^{-2}·V^{-1}·s^{-1})	κ (W·m^{-1}·K^{-1})	κ_L (W·m^{-1}·K^{-1})	Preparation	Ref.
p type											
$Pb_{0.975}Na_{0.025}S$−3%CdS	923	1.30		296	1.47	4.75	130	0.78	0.62	SSR + SPS	[98]
$Pb_{0.975}Na_{0.025}S$−3%SrS	923	1.22		221	1.70	4.55	93	0.77	0.65	SSR + SPS	[128]
$Pb_{0.99}Cu_{0.01}S$−1%Cu	773	1.20	0.79	263	2.20	2.10	470	0.85	0.65	SSR + SPS	[130]
$Pb_{0.98}Na_{0.02}S$−2%Cu_2S	823	1.20		304	1.66	2.10	164	0.89	0.72	SSR + SPS	[129]
$Pb_{0.975}Na_{0.025}S$−3%CaS	923	1.12		220	1.71	4.81	97	0.76	0.72	SSR + SPS	[128]
$Pb_{0.81}Ag_{0.16}K_{0.03}Te_{0.33}S_{0.67}$	620	~1.00		182	0.98	1.00		0.41		WC + RFIHP	[131]
n type											
$Pb_{0.93}Sb_{0.05}S_{0.5}Se_{0.5}$	900	1.70		−181	4.05	3.80	138	0.81	0.30	SSR + SPS	[132]
PbS-4.4%Ag	850	1.70		−220	4.90	3.00	90	0.79		WC + RFIHP	[133]
$Pb_{0.9}Ge_{0.1}S$	900	1.45		−315	1.16	1.48	168	0.63	0.54	SSR + SPS	[134]
$Pb_{0.985}Sb_{0.015}S$-14%GeS	923	1.32	0.76	−276	1.62	3.00	121	1.31	0.61	SSR + SPS	[135]
$Pb_{0.94}Sn_{0.06}S$−8%PbTe	923	1.30	0.72	−247	2.40	6.18	147	0.97	0.62	SSR + SPS	[99]
$Pb_{0.95}Sb_{0.02}Cu_{0.03}S$−3%Cu	923	1.23	0.62	−189	1.60	2.11	28	0.88	0.59	SSR + SPS	[136]
$Pb_{0.955}Cu_{0.045}S$	773	1.22	0.76	−275	2.05	2.52	123	0.96	0.63	WC + SPS	[137]
PbS−3%SrS−1%$PbCl_2$	930	1.20	0.78	−226	2.40	7.70	117	0.77	0.65	SSR + SPS	[138]
PbS−5%Cu	750	1.10	0.72	−248	2.10	2.10	153	1.12	0.70	WC + SPS	[139]
$Pb_{0.99}Ga_{0.01}$(S,Se,Te)	723	1.10	0.73	−254	1.97	2.35	398	1.01	0.66	WC + SPS	[140]
$Pb_{0.995}In_{0.005}S$−3%Cu	723	1.10	0.80	−226	2.60	8.40	110	1.23	0.76	SSR + SPS	[141]
PbS−3%CaS−1%$PbCl_2$	930	1.10	0.80	−234	1.65	6.30	101	0.72	0.61	SSR + SPS	[138]
PbS−1%B_2S_3−1%$PbCl_2$	923	1.10		−221	2.52			1.12	0.64	SSR + SPS	[142]
PbS Nanocrystal	838	1.06		−187	3.98	1.73	40	1.13	0.56	WC + SPS	[143]
$PbCl_{0.015}S_{0.985}$	800	1.04		−230	2.04			0.82	0.55	WC + MS	[144]
$Pb_{0.995}In_{0.005}S$−5%Ni	823	~1.00	0.66	−213	3.04	7.50	264	1.41	0.85	SSR + SPS	[145]
PbS-0.067%$PbCl_2$-1.5%Sb	823	~1.00	0.62	−223	2.56	4.50		1.13	0.74	PAS	[146]
$Pb_{0.9865}Ga_{0.0125}In_{0.001}S$	923	~1.00	0.74	−275	2.10			0.98	0.76	SSR + SPS	[100]
$Pb_{0.98}Sb_{0.02}$(S,Se,Te)	923	~1.00		−219	2.60			1.21	0.80	SSR + SPS	[147]

[b] ZT_{ave} is the average ZT in temperature ranges and PAS is plasma activated sintering respectively.

Table 3
State-of-the-art thermoelectric properties of p-type SnS-based materials.

Material	T (K)	ZT_{max}	$ZT_{ave.}$	S (μV/K)	σ (10^4 S/m)	n_H (10^{19} cm^{-3})	μ_H (cm^{-2}·V^{-1}·s^{-1})	κ (W·m^{-1}·K^{-1})	κ_L (W·m^{-1}·K^{-1})	Preparation [c]	Ref.
$SnS_{0.91}Se_{0.09}$ Crystal	873	1.60	1.25	376	0.83	2.80	310	0.69	0.51	SSR	[36]
$Sn_{0.99}Ag_{0.005}S$	877	1.10		365	0.29	0.43	3.78	0.34	0.31	MA + SPS	[148]
$Sn_{0.98}Na_{0.02}S$ Crystal	870	1.10	0.54	353	0.58	2.30	102	0.63	0.52	BM	[149]
2%hole-doped SnS Crystal	873	1.01		380	0.55	3.70	98	0.76	0.75	SSR	[150]

[c] BM is Bridgman method.

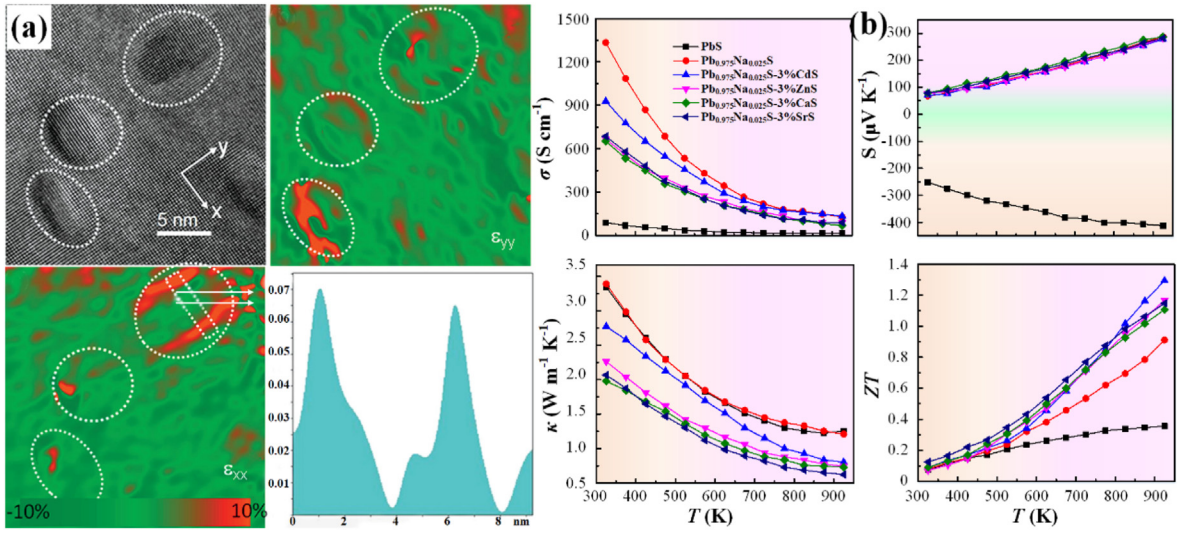

Fig. 6. (a) High resolution TEM image and stain maps of Na-doped PbS compound added by 3.0% SrS. Reprinted figure with permission from Ref. [128], Copyright 2012 by the American Chemical Society. (b) Temperature dependence of TE properties for $Pb_{0.975}Na_{0.025}S$ sample with 3.0% metal sulfides (CdS, ZnS, CaS and SrS). Adapted from Ref. [98], Copyright 2012 by the American Chemical Society.

sites can obviously elevate *n*. *ZT* values are strikingly promoted, exceeding 1.0 in Na-doped SnS crystals [150] and even reaching 1.6 after further Se alloying [36]. The TE performance in SnS crystals is superior to the polycrystalline materials.

4. New polysulfides and thermoelectric enhancement

Metal polysulfides also present a hybridized electronic band structure (particularly VB), usually deriving from M 3*d* and S 3*p* orbitals. High VB degeneracy leads to a relatively high PF. Compared with binary sulfides, polysulfides possess more complex structures, indicating a relatively larger ADPs. This may lead to the cation ion sublattice attaining a liquid-like state, with a huge impact on the κ.

4.1. Tetrahedrite

Tetrahedrite materials (based on $Cu_{12}Sb_4S_{13}$) represent two holes per formula unit, accounting for p-type metallic behavior at temperature above 85 K. They have great advantage in comparison to other state-of-the-art TE sulfides, composing of light, non-toxic elements of Cu and S. It is natural earth-abundant minerals, possibly lowering production cost. As for TE study, Suekuni *et al.* [153] firstly synthesized tetrahedrite sample and investigated its TE performance. A high $ZT = 0.15$ was received at near RT due to the decreased κ as Ni doping. Relatively, *S* displays a small value. Subsequently, considerable efforts have been directed toward improving PF through partial substitution at Cu and/or Sb sites.

General formulas of $Cu_{12-x}M6_xSb_4S_{13}$ ($0 \leq x \leq 2$) and $Cu_{12}Sb_{4-y}M7_yS_{13}$ ($0 \leq y \leq 1$) have been prepared for a wide range of substituents. M6 stands for the transition-series elements of Fe [154], Co [155,156], Ni [157], Zn [158], Mn [159], Cr [160] and Cd [161], the group of IVA elements Sn [162] and Pb [163], and the third period elements Mg [164] and Al [165]. M7 is generally Ge [166], Sn [167], Bi [168], As [169], and Te [170] elements. Table 4 presents the maximal TE properties at optimal temperature. Substitution of copper and/or antimony results in an addition of electrons based on the top of VB, altering the band degeneracy in vicinity of the E_F and further raising bandgap (E_g). Double substitution of copper [171,172] or sulfur [173] sites appears to be particularly effective in enhancing TE performance, with *ZT* values closing to or even exceeding 1.0 at their optimal temperatures. Sometimes, introduction of Se atoms [174–176] in S sites can balance the electrical and thermal transport properties. Briefly, the aim of elemental doping is to reduce *n* so that PF_{max} is well optimized and thereby receives a relatively high *ZT* value.

Introducing nanostructures into TE tetrahedrites is an effective approach for decreasing κ_L due to the strong low/middle-frequency phonon scattering. Compositional fluctuations on the endotaxial nanointerfaces between nanoregions and matrix can probably decrease the thermal transport and maintain a relatively high PF. Li's research group [38] has demonstrated a new strategy to prepare porous tetrahedrite-based TE materials with excellent electrical and thermal properties. They also have found that introducing a small amount of metallic oxide nanoparticles (NPs) into matrix achieves a significantly reduced κ, <1.1 $W \cdot m^{-1} \cdot K^{-1}$ over the entire temperatures, and thereby obtained a highest *ZT* ~1.2 at 723 K [177] (as shown in Fig. 7). These NPs include Nb_2O_5 [177], Fe_2O_3 [179], BiI_3 [38], ZnO [180], and *etc*.

4.2. Colusite

Recently, colusite-related TE materials with sphalerite-derivative structure are of interest for TE community because of their complex cationic distribution, rich crystal structure, numerus chemical active site and potential energy conversion application. Colusite family is represented by a generic formula of $Cu_{26}T_2M(8)_6S_{32}$ (T = V, Nb, Ta, Fe, Ti, Cr, Mo and W, M(8) = Sb, Ge and Sn) [54,181]. Its structure exhibits a complex cation distribution and a fascinating interplay between the corner sharing Cu–S tetrahedral network and T sites. Band structure calculation [182,183] reveals that the Fermi level penetrates into the VB manifold. The electronic states near the top of VB derive from S 3*p* and Cu 3*d* orbitals, whereas the minimum of CB is composed of T and S orbitals. A large number of atoms in a cell lower the group velocity of the optical modes and thereby reduce the heat transport efficiency by acoustic modes. It is benefit for low κ. Indeed, Suekuni *et al.* [69] first reported an extremely low κ_L value of 0.6 $W \cdot m^{-1} \cdot K^{-1}$ at 350–663 K, maintaining a relatively high PF of 6.1 $\mu W \cdot cm^{-1} \cdot K^{-2}$ at 663 K. The combination of low κ_L and relatively high PF promotes *ZT* closing to or even exceeding 1.0 at around 700 K in colusite-based $Cu_{26}V_2Sn_6S_{32}$ [67], $Cu_{26}Nb_2Ge_6S_{32}$ [68], $Cu_{26}Ta_2Sn_{5.5}S_{32}$ [68], and $[Cu_{26}Cr_2Ge_6]_{1.024}S_{32}$ [184].

4.3. Other metal based sulfides

In natural minerals, two ecofriendly elements (copper and sulfur) often appear, usually combining with other elements such as Sb, Sn, In, Ti, Bi, of Pb and transition metal elements of Mn, Fe, or Co. Most of these minerals (sulfides) do not suffer from Cu liquid-like electromigration behavior, and are considered as promising application-driven TE materials at mid-temperatures. However, they exhibit complex phases in synthesized compounds or undergo phase transitions in experimental processes, leading to a relatively low PF. These structural merits motivated great efforts to use chemical manipulation to improve TE properties of bornite [185], thiospinel [66], pavonite [186], famatinite [51], paracostibite [187], and other sphalerite-derived sulfides [188–190], in which both carrier concentration and vacancy levels were well modified. Incorporation with dehydrated attapulgite nanorods, p-type Co-

Table 4
State-of-the-art thermoelectric properties of p-type tetrahedrites.

Material	*T* (K)	ZT_{max}	*S* (μV/K)	σ (10^4 S/m)	κ ($W \cdot m^{-1} \cdot K^{-1}$)	κ_L ($W \cdot m^{-1} \cdot K^{-1}$)	Preparation	Ref.
$Cu_{11.5}Ni_{0.5}Sb_4S_{13}$-0.7%$BiI_3$	723	1.15	154	5.60	0.83	0.13	MA + SPS	[38]
$Cu_{11.5}Ni_{0.5}Sb_4S_{13}$-0.3%$Nb_2O_5$	723	1.15	172	5.40	1.20	0.36	MA + SPS	[177]
$Cu_{11}MnSb_4S_{13}$	575	1.13	142	2.60	0.26		SSR + SPS	[159]
$Cu_{13.5}Sb_4S_{12}Se$	723	1.10	177	3.90	0.81	0.22	SSR + Annealing + SPS	[174]
$Cu_{11.5}Zn_{0.5}Sb_4S_{13}$	723	1.09	247	0.78	0.31	0.18	WC + SPS	[178]
$Cu_{10.5}NiZn_{0.5}Sb_4S_{13}$	723	1.03	210	1.96	0.51	0.39	SSR + MA + CP + Annealing + HP	[171]
$Cu_{11.7}Gd_{0.3}Sb_4S_{13}$	749	~1.00	153	6.45	1.28	0.46	CP + Annealing + HP	[161]
$Cu_{11.5}Ni_{0.5}Sb_4S_{13}$–1%$Fe_2O_3$	700	~1.00	168	3.90	0.79	0.31	MA + SPS	[179]
$Cu_{12}Sb_{3.65}Sn_{0.35}S_{13}$	673	~1.00	182	3.85	0.87	0.45	CP + Annealing + MA + SPS	[167]
$Cu_{12}Sb_{3.96}Ge_{0.04}S_{13}$-0.5%ZnO	750	~1.00	152	5.28	0.93	0.25	SSR + Annealing + HP	[166]
$Cu_{11.5}Co_{0.5}Sb_4S_{13}$	673	~1.00	166	6.62	1.19	0.48	SSR + Annealing + HP	[155]
$Cu_{11.5}Co_{0.5}Sb_4S_{13}$	673	~1.00	166	5.88	1.21	0.49	SSR + CP + Anealing + HP	[156]

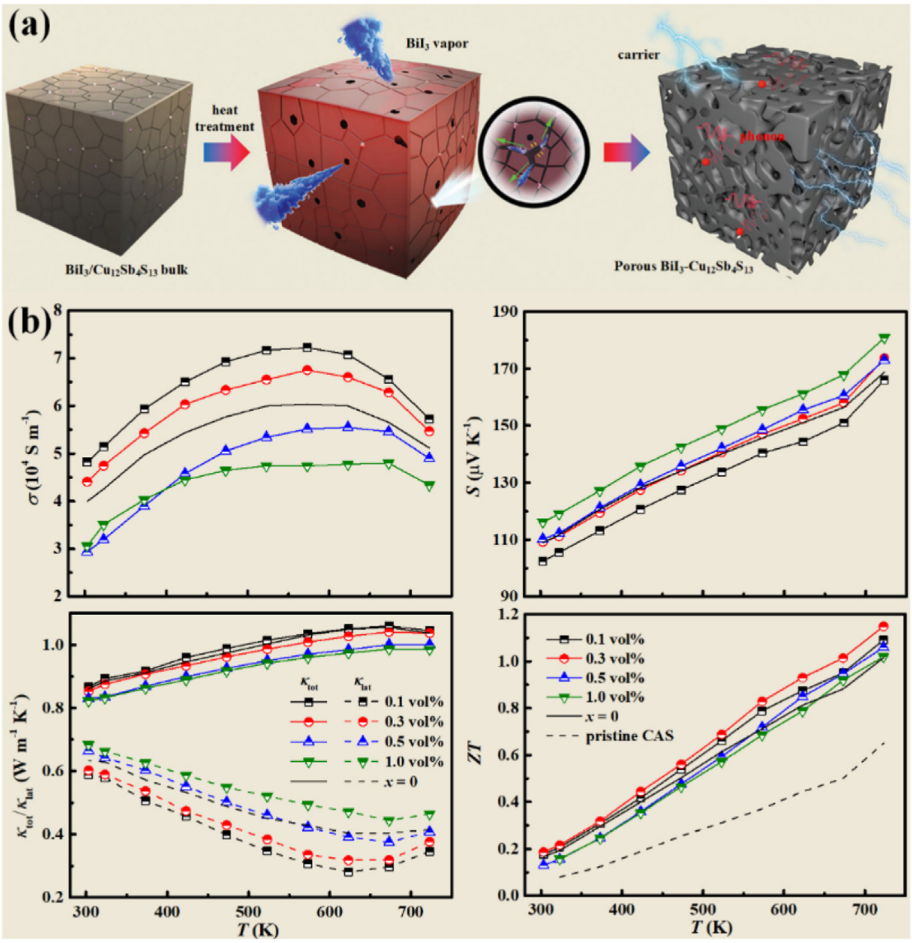

Fig. 7. (a) Schematic illustration presents the formation of $BiI_3/Cu_{12}Sb_4S_{13}$ porous composites. Reprinted figure with permission from Ref. [38], Copyright 2021 by the WILEY-VCH Verlag GmbH & Co. KGaA, Weinheim. (b) Temperature dependence of TE properties for a series of $Cu_{12}Sb_4S_{13}$-xNb_2O_5 nanocomposites. Adapted from Ref. [177], Copyright 2018 by the Elsevier Ltd.

doped $Cu_2Sn_{0.8}Co_{0.2}S_3$ [41] exhibited an enhanced *S*, high PF ~9.4 $\mu W \cdot cm^{-1} \cdot K^{-2}$, and ultralow κ_L of 0.27 $W \cdot m^{-1} \cdot K^{-1}$. Finally, a high *ZT* of ~1.0 has been achieved at 773 K. Through Br dopant-induced phase transition [43], a quasi homo-composition and hetero-structure nanocomposite based on n-type Bi_2SeS_2 provided a coherent interface and synergistically tuned electrical and thermal transport properties (ZT_{max} = 1.12@773 K). Using Cu and I as the dual carrier providers [191] suppresses the phonon transport and promotes electrical performance, and also results in an excellent *ZT* of 1.04.

5. Synthesis recipes of thermoelectric sulfides

In this short section, we review some production processes of TE sulfides. Typically, they have been synthesized by one of the following methods [192]: MA, multi-step SSR, FVIR, and bottom up method combined sintering process.

MA is a relatively rapid method, which has attracted great interests for many years in TE field. It is one of the most effective powder processing technique. Usually, the start chemicals with high purity are mixed according to nominal composition in a dry inert atmosphere, charged to an alloy jar containing balls, and set on a ball milling machine at high speed for a specific duration. The MA-derived powders are subsequently sintered by SPS or HP. Then the consolidated compounds with relatively high density are obtained. MA process gives a high-energy impact on particles involved cold-welding, fracturing and re-welding, leading to further pulverization. Therefore, it occupies an important role in TE materials, particularly in producing fine-grained composites [193], nanostructure-derived hetero-alloys [110], *in-situ* nano-defect architecture compounds [194], and *etc*. Due to the high-energy milling effect, vacancy engineering provides a huge possibility in tuning carrier concentration, effective mass and mobility, for example Ag-doped polycrystalline SnS [148]. It obtains a high PF of 4.25 $\mu W \cdot cm^{-1} \cdot K^{-2}$. Incorporating heterogeneous Cu_4SnS_4 phase [117], hole concentration was well optimized, and a reduced κ_L was achieved in $Cu_{12}Sb_4S_{13}$. Substantially, receiving an enhanced TE performance (*ZT* = 1.2@773 K). MA is greatly effective to strengthen phonon scattering and thereby significantly reduce κ. γ-Fe_2O_3-dispersed tetrahedrite [179] achieves an ultralow κ, ~0.9 $W \cdot m^{-1} \cdot K^{-1}$ over the entire temperature range, and hence leads to a high *ZT* up to 1.0, which increases by ~33%.

SSR technique is a conventional method for producing TE materials. In laboratory, typically evacuated ampoules are used to synthesize TE ingots on a gram scale. It deserves several pre-treatments including cleaning quartz tube, coating wall when volatile elements are involved, and baking probable organic residues. As followed by grounding the ingots into a fine powder, cold/hot pressed or SPS, and then annealed, the mixed start chemicals are melted in a furnace and subsequent cooling. Preparing TE materials, some post-treatments, like regulating cooling rate, are also significant in order to control the morphologies and/or crystal size

of as-synthesized ingots. It has been widely studied by various research groups, optimizing the conditions of melting, annealing and pressing procedures and investigating the promotional effects on tuning electrical and thermal transport performance. For example, Cu_2Se and Cu_2S can form a solid solution [44] using SSR method at HT to order to ensure compositional homogeneity. It possesses a unique hierarchical microstructures composed of mesoscale polymorphs, nanoscale domains and modulations. All these favorable factors lead to a much enhanced PF and yield a remarkably *ZT* value of 2.3. Jiang *et al.* [132] introduces zigzag nanoprecipitates with a uniform width of ~1.0 nm into n-type PbS-based TE material, which leads to an ultralow κ_L of 0.4 $W \cdot m^{-1} \cdot K^{-1}$. Similarly, carefully controlling the composition and reaction condition, high-quality p-type SnS crystals [36] were prepared, and show a boosted PF of 53 $\mu W \cdot cm^{-1} \cdot K^{-2}$ at RT, which achieves the highest *ZT* of 1.6@876 K.

FVIR represents a non-equilibrium synthesis technique with the advantages of rapid processing, good scalability, and energy savings. Tang's research group [195,196] systematically studied the key parameters governing the FVIR processing, and reported a wide range of FVIR-synthesized TE materials. Typically, high-purity metal powders were used as raw materials, mixed and cold-pressed into a pellet, and then sealed in a quartz tube. The FVIR process is initiated by point heating a small part of the sample. Once the ignition starts, the combustion wave passes through the remaining sample because the liberated heat of fusion in one section is sufficient to maintain the reaction in the neighboring region. The propagation of the combustion wave is fast, typically on the timescale of seconds. As FVIR-induced product is ground into powder, and then sintered again. Finally, robust TE bulks are obtained. the FVIR method could be used for the ultra-fast synthesis of metal sulfides, in which the composition could be controlled precisely. Combining FVIR with subsequent SPS process, BiAgSeS [197] multicomponent material was prepared. The non-equilibrium FVIR process provides an effective step to promote crystal grain growth and shape regular nano- and atomic-scale strain field regions at the grain boundaries. Then, the extreme low κ_L was obtained, <0.7 $W \cdot m^{-1} \cdot K^{-1}$ in the whole temperature ranges, receiving high *ZT* of 0.5 at 773 K. High purity $Cu_{1.95}S$ bulks with tunable compositions were prepared using FVIR method, and achieved a high *ZT* of 1.56 at 800 K [109].

Abovementioned processes are top down approaches to prepare TE materials, which have the feature of being somewhat energy-consuming. In order to precisely control the particle size, crystal distribution and morphology, bottom up method provides a low-cost route towards TE materials. The primary advantages lie in its versatility in designing various nanostructures, which is favorable for phonon scattering. Wet chemical synthesis provides a wide variety of nanoscaled architectures with high quality of phase purity, crystallinity, and density. For instance, PbS quantum dots (QDs) [198], the size varies from 0.5 to 5.5 nm, were successfully synthesized by an aqueous solution method. E_g can be changed by tuning synthesis parameters in order to improve TE properties. A synergized soft template-oriented attachment strategy was used to fabricate ZnS quantum wires (QWs) [199], and a typical width was only 0.8 nm. The monodisperse plasmonic and nonplasmonic I-IV-VI nanocrystals (NCs) [200] were synthesized and precisely controlled using a solvothermal method. Manipulating the chemical properties of cation precursors, the E_g of NCs decreased linearly from 2.1 to 1.2 eV MoS_2/MoO_3 hierarchical structures can be easily synthesized by hydrothermal method [201], and represented a high σ due to the zero-barrier charge injection at MoS_2/MoO_3 interface. Finally, a maximum *ZT* of 1.18 at 600 K was achieved. Core-shell-structured Cu_5FeS_4 icosahedral NPs [202] with high-density twin boundaries were synthesized by using a colloidal solution method. Orthorhombic and cubic Cu_5FeS_4 comprise the core and shell structures, respectively, exhibiting a promising *ZT* of ~0.62 at 710 K. TiS_2/C_{60} nanosheets [203] were fabricated by a solid-state reaction with a fine-grinding process, in which a competitive *ZT* of ~0.3 can be achieved at 400 K, mainly derived from the improvement of PF and reduction of κ_L. It is worth mentioning that liquid-based synthesis towards high quality TE nanomaterials still remains a challenge because of its low yield in most cases. Scale production requires automated processes with high NP contents in solution, low-cost and nontoxic precursors, solvents and surfactants, as well as the recycling side-products. Moreover, the final products usually contain some undesired impurity phases from pollution of organic solvents.

6. Conclusion and outlook

In this review, we give an overview of research progress on high-performance TE sulfides. The significant improvements and established records of *ZT* have been achieved in both n- and p-type TE alloys by carefully carrier concentration regulation, band structure manipulation, and phonon scattering. We discuss how these strategies have been validated on eco-friendly metal sulfides, including Cu–S or Cu-based, SnS, MoS_2 and Bi–S based binary sulfides and polysulfides, and lead based sulfides to improve their TE performance. In addition, materials fabrication methods and process technologies have been discussed in order to discovery new physical mechanisms, and thereby further facilitate the emergence of high-performance sulfides. Despite of colossal research progress on some potential candidates, there is still a long way to go before getting ready for commercialization.

For nanostructure-modified sulfides, the homogeneous phase dispersion is required. To avoid the solubility, especially low-dimensional inclusions, the constituent phases should be chemical, environmental, and thermal stability during the fabrication and operation processes. It will be also highly valuable for development of advanced, practical and high-performance TE technologies to understand fundamental mechanisms of electrical and thermal transport properties in nanostructured sulfides. Furthermore, it is desirable to understand the hetero-interfaces of promising sulfides at atomic scale using some advanced spectroscopic techniques, combined with insights rendered by an interatomic potential approach of first principles calculations or even machine learning.

We note that there is considerable progress on *ZT* improvement of inorganic and hybrid organic-inorganic TE materials over the past decade. However, the development of corresponding TE generators (TEGs) and modules, especially at mid to high temperature (600–1 100 K), has proceeded very slowly. To date, the number of commercially available TEGs is very small and affects only very few niche applications. These TEGs still use bismuth and lead telluride alloys. Taking $Cu_{2-x}S$ as an example, p-type parts present highly promising TE properties with $ZT = 2.3$ at 1 000 K due to high PF and intrinsically low κ_L. However, these materials show poor compatibility with other state-of-the-art n-type TE parts, which are difficult to prepare segmented modules in mid temperature ranges. Furthermore, the key technical challenges of TE $Cu_{2-x}S$ alloys, relating to the mechanical stability and the long-term chemical stability, must be maintained for at least ten years (especially on the hot generator side). This extreme environment sets maybe destroy its TEG modules. Strategies, employing electrically conductive but ion-blocking all-scale structural architectures, show that Cu ion electromigration can be effectively hindered, potentially allowing stable devices. The gap between laboratory research and device fabrication must be narrowed by reliable materials properties and well-matched electrodes and barrier materials. Good mechanical properties have rarely been addressed yet, including Vickers

hardness, fracture toughness, thermal expansion coefficient, and *etc*. Moving forward to realize widespread commercial interest, fabricating both p-type and n-type counterparts for given material needs to be taken into account. Although some binary sulfides (such as PbS and SnS) have already been researched widely, the rest are yet to be explored more.

Therefore, any breakthrough in any of the aforementioned aspects will undoubtedly be an important step forward to improve TE performance and thereby making reliable TEGs. Currently, the fabrication of commercial π-type modules is fully automated at each step and is capable of mass production. The potentials focus on Bi_2Te_3-based alloys and TE cooling (TEC) applications. Therefore, the development of stable metallized TEG legs at high temperature during operation is a problem, especially for TE sulfides, and must be mitigated or suppressed by developing effective strategies. Recent attentions, raising the toughness and fracture strength of high-*ZT* sulfides, reducing thermal expansion coefficients across the interfaces between TE materials and contact layers, developing new metal electrodes matched metal sulfides, will define the lifetime of TEGs, which will have to be of the crucial tasks for practical application. We are optimistic that future research focusing on designing better and novel TE sulfides with enhanced performance and achieving meaningful advances in broad-based TE module development.

Declaration of competing interest

The authors declare that they have no known competing financial interests or personal relationships that could have appeared to influence the work reported in this paper.

Acknowledgements

This work was supported by the National Natural Science Foundation of China, China (No. 52202232), the JST Mirai Program, Japan (No. JPMJMI19A1), the Natural Science Foundation of Hubei Province, China (No. 2022CFB937), the Guangdong Basic and Applied Basic Research Foundation, China (No. 2020A1515110251), and the CAS Key Laboratory of Cryogenics, TIPC, China (No. CRYO202204).

References

[1] Yan Q, Kanatzidis MG. High-performance thermoelectrics and challenges for practical devices. Nat Mater 2022;21(5):503–13.
[2] Freer R, Powell AV. Realising the potential of thermoelectric technology: a roadmap. J Mater Chem C 2020;8(2):441–63.
[3] Mao J, Chen G, Ren Z. Thermoelectric cooling materials. Nat Mater 2021;20(4):454–61.
[4] Hendricks T, Caillat T, Mori T. Keynote review of latest advances in thermoelectric generation materials, devices, and technologies. Energies 2022;15(19):7307.
[5] Chen W-Y, Shi X-L, Zou J, Chen Z-G. Thermoelectric coolers for on-chip thermal management: materials, design, and optimization. Mater Sci Eng R 2022;151:100700.
[6] Hu B, Shi X-L, Zou J, Chen Z-G. Thermoelectrics for medical applications: progress, challenges, and perspectives. Chem Eng J 2022;437:135268.
[7] He J, Tritt TM. Advances in thermoelectric materials research: looking back and moving forward. Science 2017;357(6358):eaak9997.
[8] Gayner C, Kar KK. Recent advances in thermoelectric materials. Prog Mater Sci 2016;83:330–82.
[9] Wei JT, Yang LL, Ma Z, Song PS, Zhang ML, Ma J, et al. Review of current high-*ZT* thermoelectric materials. J Mater Sci 2020;55(27):12642–704.
[10] Pei J, Cai B, Zhuang HL, Li JF. Bi_2Te_3-based applied thermoelectric materials: research advances and new challenges. Natl Sci Rev 2020;7(12):1856–8.
[11] Rowe DM. Thermoelectrics, an environmentally-friendly source of electrical power. Renew Energy 1999;16(1–4):1251–6.
[12] Pei Y, Shi X, LaLonde A, Wang H, Chen L, Snyder GJ. Convergence of electronic bands for high performance bulk thermoelectrics. Nature 2011;473(7345):66–9.
[13] Pei YZ, LaLonde AD, Wang H, Snyder GJ. Low effective mass leading to high thermoelectric performance. Energy Environ Sci 2012;5(7):7963–9.
[14] Li JH, Tan Q, Li JF, Liu DW, Li F, Li ZY, et al. BiSbTe-based nanocomposites with high *ZT*: the effect of SiC nanodispersion on thermoelectric properties. Adv Funct Mater 2013;23(35):4317–23.
[15] Li JF, Liu WS, Zhao LD, Zhou M. High-performance nanostructured thermoelectric materials. NPG Asia Mater 2010;2(4):152–8.
[16] Khan AU, Kobayashi K, Tang D-M, Yamauchi Y, Hasegawa K, Mitome M, et al. Nano-micro-porous skutterudites with 100% enhancement in *ZT* for high performance thermoelectricity. Nano Energy 2017;31:152–9.
[17] Zheng Z-H, Shi X-L, Ao D-W, Liu W-D, Li M, Kou L-Z, et al. Harvesting waste heat with flexible Bi_2Te_3 thermoelectric thin film. Nat Sustain 2023;6(2):180–91.
[18] Yang B, Zhang Y, Pan H, Si W, Zhang Q, Shen Z, et al. High-entropy enhanced capacitive energy storage. Nat Mater 2022;21(9):1074–80.
[19] Zhao W, Wei P, Zhang Q, Peng H, Zhu W, Tang D, et al. Multi-localization transport behaviour in bulk thermoelectric materials. Nat Commun 2015;6:6197.
[20] Zhao LD, Hao S, Lo SH, Wu CI, Zhou X, Lee Y, et al. High thermoelectric performance via hierarchical compositionally alloyed nanostructures. J Am Chem Soc 2013;135(19):7364–70.
[21] Pomrehn GS, Zevalkink A, Zeier WG, van de Walle A, Snyder GJ. Defect-controlled electronic properties in AZn_2Sb_2 Zintl phases. Angew Chem, Int Ed 2014;53(13):3422–6.
[22] Liu Z, Sato N, Gao W, Yubuta K, Kawamoto N, Mitome M, et al. Demonstration of ultrahigh thermoelectric efficiency of ~7.3% in Mg_3Sb_2/MgAgSb module for low-temperature energy harvesting. Joule 2021;5(5):1196–208.
[23] Hu L, Fang YW, Qin F, Cao X, Zhao X, Luo Y, et al. High thermoelectric performance enabled by convergence of nested conduction bands in $Pb_7Bi_4Se_{13}$ with low thermal conductivity. Nat Commun 2021;12(1):4793.
[24] Liu Z, Gao W, Oshima H, Nagase K, Lee C-H, Mori T. Maximizing the performance of n-type Mg_3Bi_2 based materials for room-temperature power generation and thermoelectric cooling. Nat Commun 2022;13(1):1120.
[25] Zhang Y, Li J, Hu WW, Yang XR, Tang XF, Tan GJ. Boosting thermoelectric performance of SnTe by selective alloying and band tuning. Mater Today Energy 2022;25:100958.
[26] Luo ZZ, Hao SQ, Zhang XM, Hua X, Cai ST, Tan GJ, et al. Soft phonon modes from off-center Ge atoms lead to ultralow thermal conductivity and superior thermoelectric performance in n-type PbSe-GeSe. Energy Environ Sci 2018;11(11):3220–30.
[27] Kim SI, Lee KH, Mun HA, Kim HS, Hwang SW, Roh JW, et al. Thermoelectrics. Dense dislocation arrays embedded in grain boundaries for high-performance bulk thermoelectrics. Science 2015;348(6230):109–14.
[28] He Y, Lu P, Shi X, Xu F, Zhang T, Snyder GJ, et al. Ultrahigh thermoelectric performance in mosaic crystals. Adv Mater 2015;27(24):3639–44.
[29] Chen Z, Jian Z, Li W, Chang Y, Ge B, Hanus R, et al. Lattice dislocations enhancing thermoelectric PbTe in addition to band convergence. Adv Mater 2017;29(23):1606768.
[30] Tan G, Shi F, Hao S, Zhao LD, Chi H, Zhang X, et al. Non-equilibrium processing leads to record high thermoelectric figure of merit in PbTe-SrTe. Nat Commun 2016;7:12167.
[31] Jiang B, Wang W, Liu S, Wang Y, Wang C, Chen Y, et al. High figure-of-merit and power generation in high-entropy GeTe-based thermoelectrics. Science 2022;377(6602):208–13.
[32] Chang C, Wu M, He D, Pei Y, Wu CF, Wu X, et al. 3D charge and 2D phonon transports leading to high out-of-plane *ZT* in n-type SnSe crystals. Science 2018;360(6390):778–83.
[33] Su L, Wang D, Wang S, Qin B, Wang Y, Qin Y, et al. High thermoelectric performance realized through manipulating layered phonon-electron decoupling. Science 2022;375(6587):1385–9.
[34] Liu X, Shi X-L, Zhang L, Liu W-D, Yang Y, Chen Z-G. One-step post-treatment boosts thermoelectric properties of PEDOT:PSS flexible thin films. J Mater Sci Technol 2023;132:81–9.
[35] Shi X-L, Liu W-D, Li M, Sun Q, Xu S-D, Du D, et al. A solvothermal synthetic environmental design for high-performance SnSe-based thermoelectric materials. Adv Energy Mater 2022;12(20):2200670.
[36] He W, Wang D, Wu H, Xiao Y, Zhang Y, He D, et al. High thermoelectric performance in low-cost $SnS_{0.91}Se_{0.09}$ crystals. Science 2019;365(6460):1418–24.
[37] Chetty R, Bali A, Mallik RC. Tetrahedrites as thermoelectric materials: an overview. J Mater Chem C 2015;3(48):12364–78.
[38] Hu H, Zhuang HL, Jiang Y, Shi J, Li JW, Cai B, et al. Thermoelectric $Cu_{12}Sb_4S_{13}$-Based synthetic minerals with a sublimation-derived porous network. Adv Mater 2021;33(43):e2103633.
[39] Hagiwara T, Suekuni K, Lemoine P, Supka AR, Chetty R, Guilmeau E, et al. Key role of d^0 and d^{10} cations for the design of semiconducting colusites: large thermoelectric *ZT* in $Cu_{26}Ti_2Sb_6S_{32}$ compounds. Chem Mater 2021;33(9):3449–56.
[40] Shi YX, Sturm C, Kleinke H. Chalcogenides as thermoelectric materials. J Solid

State Chem 2019;270:273–9.
[41] Ang R, Khan AU, Tsujii N, Takai K, Nakamura R, Mori T. Thermoelectricity generation and electron-magnon scattering in a natural chalcopyrite mineral from a deep-sea hydrothermal vent. Angew Chem, Int Ed 2015;54(44):12909–13.
[42] Tsujii N, Mori T. High Thermoelectric power factor in a carrier-doped magnetic semiconductor $CuFeS_2$. APEX 2013;6(4):043001.
[43] Jabar B, Li F, Zheng Z, Mansoor A, Zhu Y, Liang C, et al. Homo-composition and hetero-structure nanocomposite Pnma Bi_2SeS_2-Pnnm Bi_2SeS_2 with high thermoelectric performance. Nat Commun 2021;12(1):7192.
[44] Zhao KP, Qiu PF, Song QF, Blichfeld AB, Eikeland E, Ren DD, et al. Ultrahigh thermoelectric performance in $Cu_{2-y}Se_{0.5}S_{0.5}$ liquid-like materials. Mater Today Phys 2017;1:14–23.
[45] Liu H, Shi X, Xu F, Zhang L, Zhang W, Chen L, et al. Copper ion liquid-like thermoelectrics. Nat Mater 2012;11(5):422–5.
[46] Zhao YQ, Gu Y, Zong PA, Pan L, Zhang LJ, Koumoto K, et al. High thermoelectric performance of Co-doped Cu_2SnS_3-attapulgite nano-composites achieved by synergetic manipulation of electrical and thermal transport properties. J Alloys Compd 2021;887:161338.
[47] Guelou G, Kumar VP, Carnevali V, Lebedev OI, Raveau B, Couder C, et al. Long-range cationic order collapse triggered by S/Cl mixed-anion occupancy yields enhanced thermoelectric properties in $Cu_5Sn_2S_7$. Chem Mater 2021;33(23):9425–38.
[48] Deng TT, Xing T, Brod MK, Sheng Y, Qiu PF, Veremchuk I, et al. Discovery of high-performance thermoelectric copper chalcogenide using modified diffusion-couple high-throughput synthesis and automated histogram analysis technique. Energy Environ Sci 2020;13(9):3041–53.
[49] Yang YB, Ying PZ, Wang JZ, Liu XL, Du ZL, Chao YM, et al. Enhancing the thermoelectric performance of Cu_3SnS_4-based solid solutions through coordination of the Seebeck coefficient and carrier concentration. J Mater Chem 2017;5(35):18808–15.
[50] Cui J, He T, Han Z, Liu X, Du Z. Improved thermoelectric performance of solid solution $Cu_4Sn_{7.5}S_{16}$ through isoelectronic substitution of Se for S. Sci Rep 2018;8(1):8202.
[51] Shen M, Lu S, Zhang Z, Liu H, Shen W, Fang C, et al. Bi and Sn co-doping enhanced thermoelectric properties of Cu_3SbS_4 materials with excellent thermal stability. ACS Appl Mater Interfaces 2020;12(7):8271–9.
[52] Zhang JJ, Wang LJ, Liu M, Wang J, Sun K, Yang Y, et al. Preparation and thermoelectric performance of tetrahedrite-like cubic Cu_3SbS_3 compound. J Mater Sci Mater Electron 2021;32(8):10789–802.
[53] Wang H, Zheng S, Wu H, Xiong X, Xiong Q, Wang H, et al. Realizing enhanced thermoelectric performance and hardness in icosahedral $Cu_5FeS_{4-x}Se_x$ with high-density twin boundaries. Small 2022;18(2):e2104592.
[54] Zhang RZ, Chen K, Du B, Reece MJ. Screening for Cu-S based thermoelectric materials using crystal structure features. J Mater Chem 2017;5(10):5013–9.
[55] Liang D, Ma R, Jiao S, Pang G, Feng S. A facile synthetic approach for copper iron sulfide nanocrystals with enhanced thermoelectric performance. Nanoscale 2012;4(20):6265–8.
[56] Qiu XX, Qiu PF, Deng TT, Huang H, Du XL, Shi X, et al. Thermoelectric properties of nano-grained mooihoekite $Cu_9Fe_9S_{16}$. Z Anorg Allg Chem 2020;646(14):1116–21.
[57] Barbier T, Berthebaud D, Fresard R, Lebedev OI, Guilmeau E, Eyert V, et al. Structural and thermoelectric properties of n-type isocubanite $CuFe_2S_3$. Inorg Chem Front 2017;4(3):424–32.
[58] Burnett JD, Gourdon O, Ranmohotti KGS, Takas NJ, Djieutedjeu H, Poudeu PFP, et al. Structure-property relationships along the Fe-substituted $CuInS_2$ series: tuning of thermoelectric and magnetic properties. Mater Chem Phys 2014;147(1–2):17–27.
[59] Ge B, Shi Z, Zhou C, Hu J, Liu G, Xia H, et al. Enhanced thermoelectric performance of n-type eco-friendly material $Cu_{1-x}Ag_xFeS_2$ (x = 0-0.14) via bandgap tuning. J Alloys Compd 2019;809:151717.
[60] Sharma SD, Bayikadi K, Raman S, Neeleshwar S. Synergistic optimization of thermoelectric performance in earth-abundant Cu_2ZnSnS_4 by inclusion of graphene nanosheets. Nanotechnology 2020;31(36):365402.
[61] Lang YD, Pan L, Chen CC, Wang YF. Thermoelectric properties of thiospinel-type $CuCo_2S_4$. J Electron Mater 2019;48(7):4179–87.
[62] Ahn JY, Hwang JY, Ryu BK, Oh MW, Lee KH, Kim SW. Importance of crystal chemistry with interstitial site determining thermoelectric transport properties in pavonite homologue Cu-Bi-S compounds. Cryst Eng Commun 2016;18(8):1453–61.
[63] Paradis-Fortin L, Guelou G, Kumar VP, Lemoine P, Prestipino C, Merdrignac-Conanec O, et al. Structure, microstructure and thermoelectric properties of germanite-type $Cu_{22}Fe_8Ge_4S_{32}$ compounds. J Alloys Compd 2020;831:154767.
[64] Bourges C, Al Orabi RAR, Miyazaki Y. Off-stoichiometry effect on thermoelectric properties of the new p-type sulfides compounds Cu_2CoGeS_4. J Alloys Compd 2020;826:154240.
[65] Pavan Kumar V, Supka AR, Lemoine P, Lebedev OI, Raveau B, Suekuni K, et al. High power factors of thermoelectric colusites $Cu_{26}T_2Ge_6S_{32}$ (T = Cr, Mo, W): toward functionalization of the conductive "Cu-S" network. Adv Energy Mater 2018;9(6):1803249.
[66] Hashikuni K, Suekuni K, Watanabe K, Bouyrie Y, Ohta M, Ohtaki M, et al. Carrier concentration tuning in thermoelectric thiospinel $Cu_2CoTi_3S_8$ by oxidative extraction of copper. J Solid State Chem 2018;259:5–10.
[67] Bourges C, Bouyrie Y, Supka AR, Al Orabi RAR, Lemoine P, Lebedev OI, et al. High-Performance thermoelectric bulk colusite by process controlled structural disordering. J Am Chem Soc 2018;140(6):2186–95.
[68] Bouyrie Y, Ohta M, Suekuni K, Kikuchi Y, Jood P, Yamamoto A, et al. Enhancement in the thermoelectric performance of colusites $Cu_{26}A_2E_6S_{32}$ (A = Nb, Ta; E = Sn, Ge) using E-site non-stoichiometry. J Mater Chem C 2017;5(17):4174–84.
[69] Suekuni K, Kim FS, Nishiate H, Ohta M, Tanaka HI, Takabatake T. High-performance thermoelectric minerals: colusites $Cu_{26}V_2M_6S_{32}$ (M = Ge, Sn). Appl Phys Lett 2014;105(13):132107.
[70] Bourges C, Kumar VP, Nagai H, Miyazaki Y, Raveau B, Guilmeau E. Role of cobalt for titanium substitution on the thermoelectric properties of the thiospinel $CuTi_2S_4$. J Alloys Compd 2019;781:1169–74.
[71] Mangelis P, Vaqueiro P, Jumas JC, da Silva I, Smith RI, Powell AV. The effect of electron and hole doping on the thermoelectric properties of shandite-type $Co_3Sn_2S_2$. J Solid State Chem 2017;251:204–10.
[72] Wang HT, Ma HQ, Duan B, Geng HY, Zhou L, Li JL, et al. High-Pressure rapid preparation of high-performance binary silver sulfide thermoelectric materials. ACS Appl Energy Mater 2021;4(2):1610–8.
[73] He WK, Hong T, Wang DY, Gao X, Zhao LD. Low carrier concentration leads to high in-plane thermoelectric performance in n-type SnS crystals. Sci China Mater 2021;64(12):3051–8.
[74] Guo J, Yang JM, Ge ZH, Jiang BB, Qiu Y, Zhu YK, et al. Realizing high thermoelectric performance in earth-abundant Bi_2S_3 bulk materials via halogen acid modulation. Adv Funct Mater 2021;31(37):2102838.
[75] Gu Y, Song K, Hu X, Chen C, Pan L, Lu C, et al. Realization of an ultrahigh power factor and enhanced thermoelectric performance in TiS_2 via microstructural texture engineering. ACS Appl Mater Interfaces 2020;12(37):41687–95.
[76] Gautam AK, Faraz M, Khare N. Enhanced thermoelectric properties of MoS_2 with the incorporation of reduced graphene oxide (RGO). J Alloys Compd 2020;838:155673.
[77] Cai FG, Dong R, Sun W, Lei XB, Yu B, Chen J, et al. $Pb_mBi_2S_{3+m}$ homologous series with low thermal conductivity prepared by the solution-based method as promising thermoelectric materials. Chem Mater 2021;33(15):6003–11.
[78] Ohta M, Chung DY, Kunii M, Kanatzidis MG. Low lattice thermal conductivity in $Pb_5Bi_6Se_{14}$, $Pb_3Bi_2S_6$, and $PbBi_2S_4$: promising thermoelectric materials in the cannizzarite, lillianite, and galenobismuthite homologous series. J Mater Chem 2014;2(47):20048–58.
[79] Joo SJ, Ryu B, Son JH, Lee JE, Min BK, Kim BS. Highly anisotropic thermoelectric transport properties responsible for enhanced thermoelectric performance in the hot-deformed tetradymite Bi_2Te_2S. J Alloys Compd 2019;783:448–54.
[80] You YH, Su XL, Liu W, Yan YG, Fu JF, Cheng X, et al. Structure and thermoelectric property of Te doped paracostibite $CoSb_{1-x}Te_xS$ compounds. J Solid State Chem 2018;262:1–7.
[81] Telkes M. Thermoelectric power and electrical resistivity of minerals. Am Mineral 1950;35(7–8):536.
[82] Dennler G, Chmielowski R, Jacob S, Capet F, Roussel P, Zastrow S, et al. Are binary copper sulfides/selenides really new and promising thermoelectric materials? Adv Energy Mater 2014;4(9):1301581.
[83] Zhang Y, Xing C, Liu Y, Spadaro MC, Wang X, Li M, et al. Doping-mediated stabilization of copper vacancies to promote thermoelectric properties of $Cu_{2-x}S$. Nano Energy 2021;85:105991.
[84] Nam HN, Yamada R, Okumura H, Nguyen TQ, Suzuki K, Shinya H, et al. Intrinsic defect formation and the effect of transition metal doping on transport properties in a ductile thermoelectric material alpha-Ag_2S: a first-principles study. Phys Chem Chem Phys 2021;23(16):9773–84.
[85] Sun Y, Xi L, Yang J, Wu L, Shi X, Chen L, et al. The "electron crystal" behavior in copper chalcogenides Cu_2X (X = Se, S). J Mater Chem 2017;5(10):5098–105.
[86] Voneshen DJ, Walker HC, Refson K, Goff JP. Hopping time scales and the phonon-liquid electron-crystal picture in thermoelectric copper selenide. Phys Rev Lett 2017;118(14):145901.
[87] Lukashev P, Lambrecht WRL, Kotani T, Schilfgaarde VM. Electronic and crystal structure of $Cu_{2-x}S$: full-potential electronic structure calculations. Phy Rev B 2007;76(19):195202.
[88] Wang L-W. High chalcocite Cu_2S: a solid-liquid hybrid phase. Phys Rev Lett 2012;108(8):085703.
[89] Boyce JB, Huberman BA. Superionic conductors: transitions, structures, dynamics. Phys Rep 1979;51(4):189–265.
[90] He Y, Day T, Zhang T, Liu H, Shi X, Chen L, et al. High thermoelectric performance in non-toxic earth-abundant copper sulfide. Adv Mater

2014;26(23):3974–8.
[91] Shi X, Chen H, Hao F, Liu R, Wang T, Qiu P, et al. Room-temperature ductile inorganic semiconductor. Nat Mater 2018;17(5):421–6.
[92] Guin SN, Sanyal D, Biswas K. The effect of order-disorder phase transitions and band gap evolution on the thermoelectric properties of AgCuS nanocrystals. Chem Sci 2016;7(1):534–43.
[93] Kim JH, Chung DY, Bilc D, Loo S, Short J, Mahanti SD, et al. Crystal growth, thermoelectric properties, and electronic structure of $AgBi_3S_5$ and $AgSb_xBi_{3-x}S_5$ ($x = 0.3$). Chem Mater 2005;17(14):3606–14.
[94] Jiang B, Yu Y, Cui J, Liu X, Xie L, Liao J, et al. High-entropy-stabilized chalcogenides with high thermoelectric performance. Science 2021;371(6531):830–4.
[95] Liu R, Chen H, Zhao K, Qin Y, Jiang B, Zhang T, et al. Entropy as a gene-like performance indicator promoting thermoelectric materials. Adv Mater 2017;29(38):1702712.
[96] Zhang R-Z, Gucci F, Zhu H, Chen K, Reece MJ. Data-driven design of ecofriendly thermoelectric high-entropy sulfides. Inorg Chem 2018;57(20):13027–33.
[97] Pei Y, Wang H, Snyder GJ. Band engineering of thermoelectric materials. Adv Mater 2012;24(46):6125–35.
[98] Zhao L-D, He J, Hao S, Wu C-I, Hogan TP, Wolverton C, et al. Raising the thermoelectric performance of p-type PbS with endotaxial nanostructuring and valence-band offset engineering using CdS and ZnS. J Am Chem Soc 2012;134(39):16327–36.
[99] Xiao Y, Wang D, Zhang Y, Chen C, Zhang S, Wang K, et al. Band sharpening and band alignment enable high quality factor to enhance thermoelectric performance in n-type PbS. J Am Chem Soc 2020;142(8):4051–60.
[100] Luo Z-Z, Hao S, Cai S, Bailey TP, Tan G, Luo Y, et al. Enhancement of thermoelectric performance for n-type PbS through synergy of gap state and Fermi level pinning. J Am Chem Soc 2019;141(15):6403–12.
[101] Long SO, Powell AV, Hull S, Orlandi F, Tang CC, Supka AR, et al. Jahn-Teller driven electronic instability in thermoelectric tetrahedrite. Adv Funct Mater 2020;30(12):1909409.
[102] Lai W, Wang YX, Morelli DT, Lu X. From bonding asymmetry to anharmonic rattling in $Cu_{12}Sb_4S_{13}$ tetrahedrites: when lone-pair electrons are not so lonely. Adv Funct Mater 2015;25(24):3648–57.
[103] Li X, Lou Y, Jin K, Fu L, Xu P, Shi Z, et al. Realizing $ZT > 2$ in environment-friendly monoclinic Cu_2S-tetragonal $Cu_{1.96}S$ nano-phase junctions for thermoelectrics. Angew Chem, Int Ed 2022;61(45):e202212885.
[104] Zhao K, Zhu C, Qiu P, Blichfeld AB, Eikeland E, Ren D, et al. High thermoelectric performance and low thermal conductivity in $Cu_{2-y}S_{1/3}Se_{1/3}Te_{1/3}$ liquid-like materials with nanoscale mosaic structures. Nano Energy 2017;42:43–50.
[105] Zhao LL, Wang XL, Fei FY, Wang JY, Cheng ZX, Dou SX, et al. High thermoelectric and mechanical performance in highly dense $Cu_{2-x}S$ bulks prepared by a melt-solidification technique. J Mater Chem 2015;3(18):9432–7.
[106] Zhao S, Chen H, Zhao X, Luo J, Tang Z, Zeng G, et al. Excessive iodine addition leads to room-temperature superionic Cu_2S with enhanced thermoelectric properties and improved thermal stability. Mater Today Phys 2020;15:100271.
[107] Nkemeni DS, Yang Z, Lou S, Li G, Zhou S. Achievement of extra-high thermoelectric performance in doped copper sulfide. J Alloys Compd 2021;878:160128.
[108] Zhang Y-X, Lou Q, Ge Z-H, Gu S-W, Yang J-X, Guo J, et al. Excellent thermoelectric properties and stability realized in copper sulfides based composites via complex nanostructuring. Acta Mater 2022;233:117972.
[109] Yu Y, Yang D, Li J, Zhang M, Luo H, Liang Q, et al. A flash vacuum-induced reaction in preparing high performance thermoelectric Cu_2S. Adv Funct Mater 2022;32(2):2107284.
[110] Tang H, Sun F-H, Dong J-F, Asfandiyar, Zhuang H-L, Pan Y, et al. Graphene network in copper sulfide leading to enhanced thermoelectric properties and thermal stability. Nano Energy 2018;49:267–73.
[111] Mao T, Qiu P, Hu P, Du X, Zhao K, Wei T-R, et al. Decoupling thermoelectric performance and stability in liquid-like thermoelectric materials. Adv Sci 2020;7(1):1901598.
[112] Li M, Liu Y, Zhang Y, Han X, Zhang T, Zuo Y, et al. Effect of the annealing atmosphere on crystal phase and thermoelectric properties of copper sulfide. ACS Nano 2021;15(3):4967–78.
[113] Ge ZH, Chong X, Feng D, Zhang YX, Qiu Y, Xie L, et al. Achieving an excellent thermoelectric performance in nanostructured copper sulfide bulk via a fast doping strategy. Mater Today Phys 2019;8:71–7.
[114] Zheng L-J, Zhang B-P, Li HZ, Pei J, Yu J-B. Cu_xS superionic compounds: electronic structure and thermoelectric performance enhancement. J Alloys Compd 2017;722:17–24.
[115] Meng QL, Kong S, Huang ZW, Zhu YH, Liu HC, Lu XW, et al. Simultaneous enhancement in the power factor and thermoelectric performance of copper sulfide by In_2S_3 doping. J Mater Chem 2016;4(32):12624–9.
[116] Qin P, Ge Z-H, Chen Y-X, Chong X, Feng J, He J. Achieving high thermoelectric performance of $Cu_{1.8}S$ composites with WSe_2 nanoparticles. Nanotechnology 2018;29(34):345402.
[117] Tang H, Zhuang H-L, Cai B, Asfandiyar, Dong J, Sun F-H, et al. Enhancing the thermoelectric performance of $Cu_{1.8}S$ by Sb/Sn co-doping and incorporating multiscale defects to scatter heat-carrying phonons. J Mater Chem C 2019;7(14):4026–31.
[118] Liu W-D, Shi X-L, Gao H, Moshwan R, Xu S-D, Wang Y, et al. Kinetic condition driven phase and vacancy enhancing thermoelectric performance of low-cost and eco-friendly $Cu_{2-x}S$. J Mater Chem C 2019;7(18):5366–73.
[119] Ge Z-H, Liu X, Feng D, Lin J, He J. High-performance thermoelectricity in nanostructured earth-abundant copper sulfides bulk materials. Adv Energy Mater 2016;6(16):1600607.
[120] Luo H, Yang D, Yu Y, Liang Q, Peng H, Xia F, et al. The high-pressure processed Cu_2S: phase intergrowth with strained lamella leading to an improved thermoelectric performance. Adv Electron Mater 2022;8(2):2100835.
[121] Yang D, Su X, Yan Y, He J, Uher C, Tang X. Mechanochemical synthesis of high thermoelectric performance bulk Cu_2X (X = S, Se) materials. Apl Mater 2016;4(11):116110.
[122] Chen X, Zhang H, Zhao Y, Liu W-D, Dai W, Wu T, et al. Carbon-encapsulated copper sulfide leading to enhanced thermoelectric properties. ACS Appl Mater Interfaces 2019;11(25):22457–63.
[123] Tang Y-Q, Zhang K, Ge Z-H, Feng J. Facile synthesis and thermoelectric properties of $Cu_{1.96}S$ compounds. J Solid State Chem 2018;265:140–7.
[124] Zhang Y-X, Zhu Y-K, Feng J, Ge Z-H. Precious metal nanoparticles dispersing toward highly enhanced mechanical and thermoelectric properties of copper sulfides. J Alloys Compd 2022:892162035.
[125] Chen X-Q, Fan S-J, Han C, Wu T, Wang L-J, Jiang W, et al. Multiscale architectures boosting thermoelectric performance of copper sulfide compound. Rare Met 2021;40(8):2017–25.
[126] Mikula A, Nieroda P, Mars K, Dabrowa J, Kolezynski A. Structural, thermoelectric and stability studies of Fe-doped copper sulfide. Solid State Ionics 2020;350:115322.
[127] Liu HL, Shi X, Xu FF, Zhang LL, Zhang WQ, Chen LD, et al. Copper ion liquid-like thermoelectrics. Nat Mater 2012;11(5):422–5.
[128] Zhao L-D, He J, Wu C-I, Hogan TP, Zhou X, Uher C, et al. Thermoelectrics with earth abundant elements: high performance p-type PbS nanostructured with SrS and CaS. J Am Chem Soc 2012;134(18):7902–12.
[129] Qin Y, Xiao Y, Wang D, Qin B, Huang Z, Zhao L-D. An approach of enhancing thermoelectric performance for p-type PbS: decreasing electronic thermal conductivity. J Alloys Compd 2020;820:153453.
[130] Qin Y, Hong T, Qin B, Wang D, He W, Gao X, et al. Contrasting Cu roles lead to high ranged thermoelectric performance of PbS. Adv Funct Mater 2021;31(34):2102185.
[131] Ibanez M, Genc A, Hasler R, Liu Y, Dobrozhan O, Nazarenko O, et al. Tuning transport properties in thermoelectric nanocomposites through inorganic ligands and heterostructured building blocks. ACS Nano 2019;13(6):6572–80.
[132] Jiang B, Liu X, Wang Q, Cui J, Jia B, Zhu Y, et al. Realizing high-efficiency power generation in low-cost PbS-based thermoelectric materials. Energy Environ Sci 2020;13(2):579–91.
[133] Ibanez M, Luo Z, Genc A, Piveteau L, Ortega S, Cadavid D, et al. High-performance thermoelectric nanocomposites from nanocrystal building blocks. Nat Commun 2016;7:10766.
[134] Rathore E, Juneja R, Sarkar D, Roychowdhury S, Kofu M, Nakajima K, et al. Enhanced covalency and nanostructured-phonon scattering lead to high thermoelectric performance in n-type PbS. Mater Today Energy 2022;24:100953.
[135] Luo Z-Z, Cai S, Hao S, Bailey TP, Xie H, Slade TJ, et al. Valence disproportionation of GeS in the PbS matrix forms $Pb_5Ge_5S_{12}$ inclusions with conduction band alignment leading to high n-type thermoelectric performance. J Am Chem Soc 2022;144(16):7402–13.
[136] Zhao M, Chang C, Xiao Y, Gu R, He J, Zhao L-D. Investigations on distinct thermoelectric transport behaviors of Cu in n-type PbS. J Alloys Compd 2019;781:820–30.
[137] Li M, Liu Y, Zhang Y, Chang C, Zhang T, Yang D, et al. Room temperature aqueous-based synthesis of copper-doped lead sulfide nanoparticles for thermoelectric application. Chem Eng J 2022;433:133837.
[138] Hou Z, Qiu Y, Ren D, Huang Z, Zhao L-D. Enhancing thermoelectric transport properties of n-type PbS through introducing CaS/SrS. J Solid State Chem 2019;280:130–8.
[139] Li M, Liu Y, Zhang Y, Han X, Xiao K, Nabahat M, et al. PbS-Pb-Cu_xS composites for thermoelectric application. ACS Appl Mater Interfaces 2021;13(43):51373–82.
[140] Cheng R, Wang D, Bai H, Wu J, Liu W, Zhao L-D, et al. Bridging the miscibility gap towards higher thermoelectric performance of PbS. Acta Mater 2021;220:117337.
[141] Hou Z, Wang D, Hong T, Qin Y, Peng S, Wang G, et al. Boosting thermoelectric

performance of n-type PbS through synergistically integrating in resonant level and Cu dynamic doping. J Phys Chem Solid 2021;148:109640.
[142] Zhao L-D, Lo S-H, He J, Li H, Biswas K, Androulakis J, et al. High performance thermoelectrics from earth-abundant materials: enhanced figure of merit in PbS by second phase nanostructures. J Am Chem Soc 2011;133(50):20476–87.
[143] Xu B, Feng T, Li Z, Pantelides ST, Wu Y. Constructing highly porous thermoelectric monoliths with high-performance and improved portability from solution-synthesized shape-controlled nanocrystals. Nano Lett 2018;18(6):4034–9.
[144] Du X, Wang Y, Shi R, Mao Z, Yuan Z. Effects of anion and cation doping on the thermoelectric properties of n-type PbS. J Eur Ceram Soc 2018;38(10):3512–7.
[145] Hou Z, Hong T, Wang D, Gao X, Qiu Y, Zhao L-D. Contrasting thermoelectric transport properties of n-type PbS induced by adding Ni and Zn. ACS Appl Energy Mater 2021;4(6):6284–9.
[146] Yang J, Zhang X, Liu G, Zhao L, Liu J, Shi Z, et al. Multiscale structure and band configuration tuning to achieve high thermoelectric properties in n-type PbS bulks. Nano Energy 2020;74:104826.
[147] Zhao M, Chang C, Xiao Y, Zhao L-D. High performance of n-type $(PbS)_{1-x-y}(PbSe)_x(PbTe)_y$ thermoelectric materials. J Alloys Compd 2018;744:769–77.
[148] Asfandiyar, Cai B, Zhao L-D, Li J-F. High thermoelectric figure of merit $ZT > 1$ in SnS polycrystals. J Materiomics 2020;6(1):77–85.
[149] Wu H, Lu X, Wang G, Peng K, Chi H, Zhang B, et al. Sodium-doped tin sulfide single crystal: anontoxic earth-abundant material with high thermoelectric performance. Adv Energy Mater 2018;8(20):1800087.
[150] He W, Wang D, Dong J-F, Qiu Y, Fu L, Feng Y, et al. Remarkable electron and phonon band structures lead to a high thermoelectric performance $ZT > 1$ in earth-abundant and eco-friendly SnS crystals. J Mater Chem 2018;6(21):10048–56.
[151] Tan Q, Li J-F. Thermoelectric properties of Sn-S bulk materials prepared by mechanical alloying and spark plasma sintering. J Electron Mater 2014;43(6):2435–9.
[152] Tang H, Dong J-F, Sun F-H, Asfandiyar, Shang P, Li J-F. Adjusting Na doping via wet-chemical synthesis to enhance thermoelectric properties of polycrystalline SnS. Sci China Mater 2019;62(7):1005–12.
[153] Suekuni K, Tsuruta K, Ariga T, Koyano M. Thermoelectric properties of mineral tetrahedrites $Cu_{10}Tr_2Sb_4S_{13}$ with low thermal conductivity. APEX 2012;5(5):051201.
[154] Weller DP, Kunkel GE, Ochs AM, Morelli DT, Anderson ME. Observation of n-type behavior in Fe-doped tetrahedrite at low temperature. Mater Today Phys 2018;7:1–6.
[155] Tippireddy S, Chetty R, Naik MH, Jain M, Chattopadhyay K, Mallik RC. Electronic and thermoelectric properties of transition metal substituted tetrahedrites. J Phys Chem C 2018;122(16):8735–49.
[156] Chetty R, Bali A, Naik MH, Rogl G, Rogl P, Jain M, et al. Thermoelectric properties of Co substituted synthetic tetrahedrite. Acta Mater 2015;100:266–74.
[157] Suekuni K, Tsuruta K, Kunii M, Nishiate H, Nishibori E, Maki S, et al. High-performance thermoelectric mineral $Cu_{12-x}Ni_xSb_4S_{13}$ tetrahedrite. J Appl Phys 2013;113(4):043712.
[158] Harish S, Sivaprahasam D, Battabyal M, Gopalan R. Phase stability and thermoelectric properties of $Cu_{10.5}Zn_{1.5}Sb_4S_{13}$ tetrahedrite. J Alloys Compd 2016;667:323–8.
[159] Heo J, Laurita G, Muir S, Subramanian MA, Keszler DA. Enhanced thermoelectric performance of synthetic tetrahedrites. Chem Mater 2014;26(6):2047–51.
[160] Kumar DSP, Tippireddy S, Ramakrishnan A, Chen K-H, Malar P, Mallik RC. Thermoelectric and electronic properties of chromium substituted tetrahedrite. Semicond Sci Technol 2019;34(3):035017.
[161] Zhu C, Chen Q, Ming H, Qin X, Yang Y, Zhang J, et al. Improved thermoelectric performance of $Cu_{12}Sb_4S_{13}$ through Gd-substitution induced enhancement of electronic density of states and phonon scattering. ACS Appl Mater Interfaces 2021;13(21):25092–101.
[162] Goto Y, Sakai Y, Kamihara Y, Matoba M. Effect of Sn-substitution on thermoelectric properties of copper-based sulfide, famatinite Cu_3SbS_4. J Phys Soc Jpn 2015;84(4):044706.
[163] Huang LL, Wang YS, Zhu C, Xu R, Li JM, Zhang JH, et al. Preparation and enhanced thermoelectric performance of Pb-doped tetrahedrite $Cu_{12-x}Pb_xSb_4S_{13}$. J Alloys Compd 2018;769:478–83.
[164] Levinsky P, Candolfi C, Dauscher A, Lenoir B, Hejtmanek J. Thermoelectric properties of magnesium-doped tetrahedrite $Cu_{12-x}Mg_xSb_4S_{13}$. J Electron Mater 2019;48(4):1926–31.
[165] Tippireddy S, Ghosh S, Biswas R, Dasgupta T, Rogl G, Rogl P, et al. Thermoelectric properties of Al substituted tetrahedrite. J Appl Phys 2020;127(3):035105.
[166] Huang L, Kong Y, Zhang J, Xu R, Zhu C, Wu J, et al. Achieving a high thermoelectric performance of tetrahedrites by adjusting the eelectronic density of states and enhancing phonon scattering. ACS Appl Mater Interfaces 2019;11(26):23361–71.
[167] Tippireddy S, Kumar DSP, Karati A, Ramakrishnan A, Sarkar S, Peter SC, et al. Effect of Sn substitution on the thermoelectric properties of synthetic tetrahedrite. ACS Appl Mater Interfaces 2019;11(24):21686–96.
[168] Kumar DSP, Chetty R, Femi OE, Chattopadhyay K, Malar P, Mallik RC. Thermoelectric properties of Bi doped tetrahedrite. J Electron Mater 2017;46(5):2616–22.
[169] Levinsky P, Candolfi C, Dauscher A, Tobola J, Hejtmanek J, Lenoir B. Thermoelectric properties of the tetrahedrite-tennantite solid solutions $Cu_{12}Sb_{4-x}As_xS_{13}$ and $Cu_{10}Co_2Sb_{4-y}As_yS_{13}$ ($0 < x = y < 4$). Phys Chem Chem Phys 2019;21(8):4547–55.
[170] Bouyrie Y, Candolfi C, Ohorodniichuk V, Malaman B, Dauscher A, Tobola J, et al. Crystal structure, electronic band structure and high-temperature thermoelectric properties of Te-substituted tetrahedrites $Cu_{12}Sb_{4-x}Te_xS_{13}$ ($0.5 < x < 2.0$). J Mater Chem C 2015;3(40):10476–87.
[171] Lu X, Morelli DT, Xia Y, Ozolins V. Increasing the thermoelectric figure of merit of tetrahedrites by Co-doping with nickel and zinc. Chem Mater 2015;27(2):408–13.
[172] Weller DP, Morelli DT. Rapid synthesis of zinc and nickel co-doped tetrahedrite thermoelectrics by reactive spark plasma sintering and mechanical alloying. J Alloys Compd 2017;710:794–9.
[173] Rout U, Tippireddy S, Werbach K, Pambannan P, Rogl G, Rogl P, et al. Simultaneous optimization of power factor and thermal conductivity via Te and Se double substitution in $Cu_{12}Sb_4S_{13}$ tetrahedrite. Scripta Mater 2020;188:151–6.
[174] Yan Y, Wu H, Wang G, Lu X, Zhou X. High thermoelectric performance balanced by electrical and thermal transport in tetrahedrites $Cu_{12+x}Sb_4S_{12}Se$. Energy Storage Mater 2018;13:127–33.
[175] Lu X, Yao W, Wang GW, Zhou XY, Morelli D, Zhang YS, et al. Band structure engineering in highly degenerate tetrahedrites through isovalent doping. J Mater Chem 2016;4(43):17096–103.
[176] Lu X, Morelli DT, Wang YX, Lai W, Xia Y, Ozolins V. Phase stability, crystal structure, and thermoelectric properties of $Cu_{12}Sb_4S_{13-x}Se_x$ solid solutions. Chem Mater 2016;28(6):1781–6.
[177] Sun F-H, Dong J, Tang H, Shang P-P, Zhuang H-L, Hu H, et al. Enhanced performance of thermoelectric nanocomposites based on $Cu_{12}Sb_4S_{13}$ tetrahedrite. Nano Energy 2019;57:835–41.
[178] Weller DP, Stevens DL, Kunkel GE, Ochs AM, Holder CF, Morelli DT, et al. Thermoelectric performance of tetrahedrite synthesized by a modified polyol process. Chem Mater 2017;29(4):1656–64.
[179] Hu HH, Sun FH, Dong JF, Zhuang HL, Cai BW, Pei J, et al. Nanostructure engineering and performance enhancement in Fe_2O_3-dispersed $Cu_{12}Sb_4S_{13}$ thermoelectric composites with earth-abundant elements. ACS Appl Mater Interfaces 2020;12(15):17864–72.
[180] Sun F-H, Dong J, Tang H, Zhuang H-L, Li J-F. ZnO-nanoparticle-dispersed $Cu_{11.5}Ni_{0.5}Sb_4S_{13-\delta}$ tetrahedrite composites with enhanced thermoelectric performance. J Electron Mater 2019;48(4):1840–5.
[181] Kumar VP, Guelou G, Lemoine P, Raveau B, Supka AR, Al Orabi RAR, et al. Copper-rich thermoelectric dulfides: size-mismatch effect and chemical disorder in the TS_4Cu_6 complexes of $Cu_{26}T_2Ge_6S_{32}$ (T = Cr, Mo, W) colusites. Angew Chem, Int Ed 2019;58(43):15455–63.
[182] Kumar VP, Mitra S, Guelou G, Supka AR, Lemoine P, Raveau B, et al. Transport properties and electronic density-of-states of Zn-doped colusite $Cu_{26}Cr_2Ge_6S_{32}$. Appl Phys Lett 2020;117(17):173902.
[183] Kim FS, Suekuni K, Nishiate H, Ohta M, Tanaka HI, Takabatake T. Tuning the charge carrier density in the thermoelectric colusite. J Appl Phys 2016;119(17):175105.
[184] Guelou G, Kumar VP, Bourhim A, Lemoine P, Raveau B, Supka A, et al. Toppling the transport properties with cationic overstoichiometry in thermoelectric colusite: $Cu_{26}Cr_2Ge_{6(1+delta)}S_{32}$. ACS Appl Energy Mater 2020;3(5):4180–5.
[185] Guo L, Zhang B, Zhu H, Wu H, Yan Y, Gong X, et al. Manipulating the phase transformation temperature to achieve cubic $Cu_5FeS_{4-x}Se_x$ and enhanced thermoelectric performance. J Mater Chem C 2020;8(48):17222–8.
[186] Hwang J-Y, Ahn JY, Lee KH, Kim SW. Structural optimization for thermoelectric properties in Cu-Bi-S pavonite compounds. J Alloys Compd 2017;704:282–8.
[187] You Y, Su X, Liu W, Yan Y, Fu J, Cheng X, et al. Structure and thermoelectric property of Te doped paracostibite $CoSb_{1-x}Te_xS$ compounds. J Solid State Chem 2018;262:1–7.
[188] Gu Y, Ai W, Zhao Y, Pan L, Lu C, Zong P, et al. Remarkable thermoelectric property enhancement in Cu_2SnS_3-$CuCo_2S_4$ nanocomposites via 3D modulation doping. J Mater Chem 2021;9(31):16928–35.
[189] Saxena M, Tarachand, Bera AK, Okram GS. Impact of non-stoichiometry in the thermoelectric performance of polyol method prepared $Cu_{1+x}In_{1-x}S_2$ ($x =$

-0.3,-0.2,-0.1, 0, 0.1, 0.2) nanowires. J Alloys Compd 2021;881:160517.
[190] Labegorre J-B, Virfeu A, Bourhim A, Willeman H, Barbier T, Appert F, et al. XBi_4S_7 (X = Mn, Fe): new cost-efficient layered n-type thermoelectric sulfides with ultralow thermal conductivity. Adv Funct Mater 2019;29(48):1904112.
[191] Li F, Ruan M, Jabar B, Liang C, Chen Y, Ao D, et al. High thermoelectric properties achieved in environmentally friendly sulfide compound Bi_2SeS_2 by nanoenginnering. Nano Energy 2021;88:106273.
[192] Li J, Pan Y, Wu C, Sun F, Wei T. Processing of advanced thermoelectric materials. Sci China Technol Sci 2017;60(9):1347–64.
[193] Li Z-Y, Li J-F. Fine-grained and nanostructured $AgPb_mSbTe_{m+2}$ alloys with high thermoelectric figure of merit at medium temperature. Adv Energy Mater 2014;4(2):201300937.
[194] Jiang Y, Dong J, Zhuang H-L, Yu J, Su B, Li H, et al. Evolution of defect structures leading to high *ZT* in GeTe-based thermoelectric materials. Nat Commun 2022;13(1):6087.
[195] Su X, Fu F, Yan Y, Zheng G, Liang T, Zhang Q, et al. Self-propagating high-temperature synthesis for compound thermoelectrics and new criterion for combustion processing. Nat Commun 2014;5:4908.
[196] Su X, Wei P, Li H, Liu W, Yan Y, Li P, et al. Multi-scale microstructural thermoelectric materials: transport behavior, non-equilibrium preparation, and applications. Adv Mater 2017;29(20):1602013.
[197] Yang D, Luo T, Su X, Wu J, Tang X. Unveiling the intrinsic low thermal conductivity of BiAgSeS through entropy engineering in SHS kinetic process. J Inorg Mater 2021;36(9):991–8.
[198] Das P, Claverie JP. Synthesis of single-core and multiple-core core-shell nanoparticles by RAFT emulsion polymerization: lead sulfide-copolymer nanocomposites. J Polym Sci, Polym Chem Ed 2012;50(14):2802–8.
[199] Li D, Hao S, Xing G, Li Y, Li X, Fan L, et al. Solution grown single-unit-cell quantum wires affording self-powered solar-blind UV photodetectors with ultrahigh selectivity and sensitivity. J Am Chem Soc 2019;141(8):3480–8.
[200] Wang XL, Swihart MT. Controlling the size, shape, phase, band gap, and localized surface plasmon resonance of $Cu_{2-x}S$ and Cu_xIn_yS nanocrystals. Chem Mater 2015;27(5):1786–91.
[201] Abinaya R, Harish S, Ponnusamy S, Shimomura M, Navaneethan M, Archana J. Enhanced thermoelectric figure-of-merit of MoS_2/α-MoO_3 nanosheets via tuning of sulphur vacancies. Chem Eng J 2021;416:128484.
[202] Zhang A, Zhang B, Lu W, Xie D, Ou H, Han X, et al. Twin engineering in wolution-wynthesized nonstoichiometric Cu_5FeS_4 icosahedral nanoparticles for enhanced thermoelectric performance. Adv Funct Mater 2018;28(10):1705117.
[203] Wang L, Zhang Z, Geng L, Yuan T, Liu Y, Guo J, et al. Solution-printable fullerene/TiS_2 organic/inorganic hybrids for high-performance flexible n-type thermoelectrics. Energy Environ Sci 2018;11(5):1307–17.

Fu-Hua Sun is currently an associate professor of School of Materials Science and Engineering at Hubei Normal University, China. He received his Ph.D. degree from Tsinghua University in 2019. He worked as a postdoctoral research fellow at Wuhan University of Technology (2020–2022). His current research focuses on the synthesis of nano-bulk sulfur-based materials and their applications in thermoelectric.

Hezhang Li received his Ph.D. degree from Tohoku University, Japan in 2022 and then worked in National Institute for Materials Science (NIMS), Japan as a postdoc researcher from April 2022 to February 2023. He is now a postdoctoral researcher at Tsinghua University, China. His research focuses on the calculation of electronic structure, crystal structure analysis and the transport properties of Heusler alloys and other thermoelectric materials.

Takao Mori is a professor at NIMS & University of Tsukuba, Tsukuba, Japan. Prof. Mori's present research fields focus on Thermoelectrics, Magnetism, Solid State Physics, Inorganic Materials Science, and Material Synthesis. He is particularly interested in inorganic compounds with "network" structures; atomic clusters, cages, and nets. One particular focus is to develop thermoelectric materials viable for the first wide scale applications. From 2010 Prof. Mori has been a Visiting Professor at Hiroshima University, and Adj. Prof. at Univ. of Tsukuba. Prof. Mori is also Lab Director of the NIMS Open Innovation Center (NOIC), Thermal Energy Conversion Lab, which is a multicompany and institute open innovation endeavor carrying out challenging research on thermoelectrics.